TECTONICS, VOL. 32, 1227–1246, doi:10.1002/tect.20076, 2013

Fault weakening across the frictional-viscous transition zone, Karakoram Fault Zone, NW Himalaya

David Wallis,[1] Richard J. Phillips,[1] and Geoffrey E. Lloyd [1]

Received 17 December 2012; revised 13 August 2013; accepted 21 August 2013; published 1 October 2013.

[1] Exhumed fault rocks formed in the frictional-viscous transition zone (FVTZ) provide test material that can be used to assess the strength of natural fault zones. In the Karakoram Fault Zone (KFZ), such rocks contain evidence of several long-term weakening mechanisms associated with reduced coefficients of friction (<0.4). The Nubra, Tangtse, and Arganglas strands of the KFZ are focused along metavolcano-sedimentary formations indicating weakness relative to the bounding granitoids. Synkinematic retrogression suggests that reaction softening has weakened the margins of granitoids along the Nubra and Tangtse strands and the Nubra Formation within the Nubra strand. The resultant phyllosilicates have formed well-developed interconnected weak layers within phyllonites and granitic mylonites. Micaceous foliae with increased proportions of opaque minerals in granitic mylonites suggest that fluid-assisted diffusive mass transfer aided deformation within the Nubra and Tangtse strands. Microstructures within Nubra strand phyllonites suggest that frictional-viscous flow accommodated deformation at low shear stresses in the FVTZ. Multiple generations of veining within each strand indicate overpressured pore fluids within the fault zone across a range of depths. Active springs and travertines along the fault indicate ongoing suprahydrostatic fluid flow within the KFZ. Despite such evidence for weakening mechanisms, the KFZ is currently locked and most likely generates moment magnitude 7.5+ earthquakes. Evidence for multiple fault weakening mechanisms reduces potential for shear heating within the KFZ and suggests that the long-term strength of the lithosphere must reside below the depth of penetration of the fault.

Citation: Wallis, D., R. J. Phillips, and G. E. Lloyd (2013), Fault weakening across the frictional-viscous transition zone, Karakoram Fault Zone, NW Himalaya, *Tectonics*, *32*, 1227–1246, doi:10.1002/tect.20076.

1. Introduction

[2] Investigating the frictional strength of fault zones is critical to determining their slip stability [*Ikari et al*., 2011] and to characterizing the micro- to macroscopic deformation of the continental lithosphere [*Rutter et al*., 2001]. Relative weakness between fault zones and intact crust, or between lithologies of differing rheologies, can be inferred on the basis of strain localization into the weaker material. However, it is also pertinent to determine whether faults are weak in an absolute sense, i.e., able to deform at shear stresses significantly lower than those possible for dry rock with a Byerlee coefficient of friction (μ) in the range 0.6–0.85 [*Byerlee*, 1978]. Absolute weakness may occur when the rock deforms with lower values of μ or when elevated pore fluid pressures reduce the effective normal stress, thus enabling slip at low shear stresses. Such absolute weakness may be inferred on the basis of relating observed deformation fabrics and microstructures to experimental or modeled results of weakening mechanisms that reduce frictional strength.

[3] Whilst the crust outside major fault zones has been shown to be strong [*Townend and Zoback*, 2000; *Zoback and Harjes*, 1997], evidence for the absolute weakness of several major faults has been put forward. These include strike-slip faults such as the Punchbowl/North Branch San Gabriel Faults, California [*Chester and Logan*, 1986; *Chester and Chester*, 1998; *Wilson et al*., 2003], Carboneras Fault, Spain [*Faulkner et al*., 2003], Great Glen Fault Zone, Scotland [*Stewart et al*., 2000], Median Tectonic Line, Japan [*Jefferies et al*., 2006a, 2006b], and Alpine Fault Zone, New Zealand [*Barth et al*., 2013; *White and White*, 1983], as well as low-angle normal faults such as the Zuccale Fault, Elba [*Collettini et al*., 2006].

[4] In the India-Asia collision zone, large-scale fault zones are abundant (Figure 1 insert). However, despite their considerable seismogenic potential, their significance for understanding the evolution of the Himalayan-Tibetan orogen [*Searle et al*., 2011], and widespread interest in the macroscopic strength of the lithosphere in the region [e.g., *Cook and Royden*, 2008; *Jackson*, 2002], no geological studies have yet investigated the absolute strength of fault rocks formed at depth in these structures. The strength of fault zones can also impact processes such as shear heating [*Leloup et al*., 1999] and metamorphism [*Steffen et al*.,

[1]School of Earth and Environment, University of Leeds, Leeds, UK.

Corresponding author: D. Wallis, School of Earth and Environment, University of Leeds, Leeds LS2 9JT, UK. (eedw@leeds.ac.uk)

0278-7407/13/10.1002/tect.20076

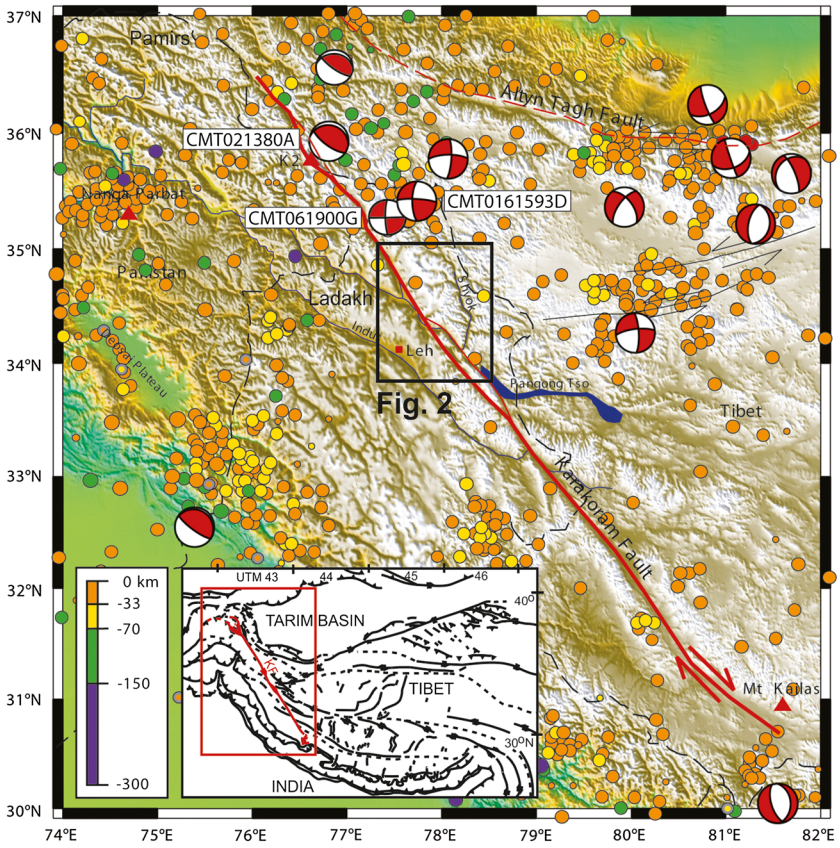

Figure 1. The Karakoram Fault Zone (KFZ) with Harvard Centroid Moment Tensor (CMT) solutions, International Seismological Centre and National Earthquake Information Centre data and historic earthquakes during the period 1964–2003. Body wave magnitudes ranged from 3.0 to 5.3 for the ISC/NEIC data and 4.5 to 6.5 for the Harvard CMT data. Insert shows location of main figure. The KFZ has been largely seismically inactive during the 40 year recording period. Earthquake CMT021380A has a depth of 80 km and may be associated with transpression in the vicinity of K2. CMT061900G and CMT0161593D may result from dextral slip on a slightly contorted Karakoram fault plane striking 179°–188°, but equally could be associated with widespread sinistral strike-slip faulting in the northern Tibetan plateau. The black box marks the study area shown in Figure 2.

2001] within them, which can in turn also affect the fault strength. In this study, we investigate deformation microstructures preserved in fault rocks from one of the most prominent faults in the India-Asia collision zone, the Karakoram Fault Zone (KFZ). We describe evidence for the operation of various deformation mechanisms, interpret the operative fault weakening processes, and then explore their implications for seismicity, shear heating, and continental lithospheric strength.

[5] Large-scale fault zones can contain a wide range of fault rocks formed by a variety of deformation processes. In order to describe and distinguish between these processes and their products, we use the following definitions: the terms brittle and ductile are used to describe fault rocks/fabrics that, respectively, display or lack significant discontinuities at the scale of observation. We reserve the terms frictional and viscous to describe the interpreted deformation mechanism.

[6] Central to determining the frictional strength of faults is the identification of potential fault weakening mechanisms and the recognition of evidence for their presence within fault zones [*Imber et al*., 2008]. A broad range of potential weakening processes have been recognized that may variably impact fault strength over a range of depths and timescales. Key weakening mechanisms proposed to operate in the upper crust within large displacement faults include the presence of low-friction phyllosilicate-rich fault gouges [*Boulton et al*., 2012; *Morrow et al*., 2000; *Saffer et al*., 2001; *Scholz*, 1998], elevated pore fluid pressures [*Smith et al*., 2008], and frictional-viscous flow within phyllonitic fault rocks [*Bos and Spiers,* 2001; *Bos and Spiers*, 2002; *Chester*, 1995; *Chester and Higgs*, 1992; *Holdsworth*, 2004; *Niemeijer and Spiers*, 2005]. Additionally, processes such as grain size reduction [*De Bresser et al*., 2001], reaction weakening [*Wintsch et al*., 1995], thermal perturbations, and the addition of melt [*Leloup et al*., 1999] may weaken fault rocks, particularly in the deeper portions of fault zones. A separate category of dynamic weakening processes has been suggested to occur during the coseismic interval and include fault lubrication [*Di Toro et al*., 2011] and thermal pressurization [*Wibberley and Shimamoto*, 2005].

[7] In order to investigate fault strength and deformation processes over a broad range of upper-midcrustal depths, together with their evolution over geological time, it is necessary to investigate exhumed fault zones that exhibit fault

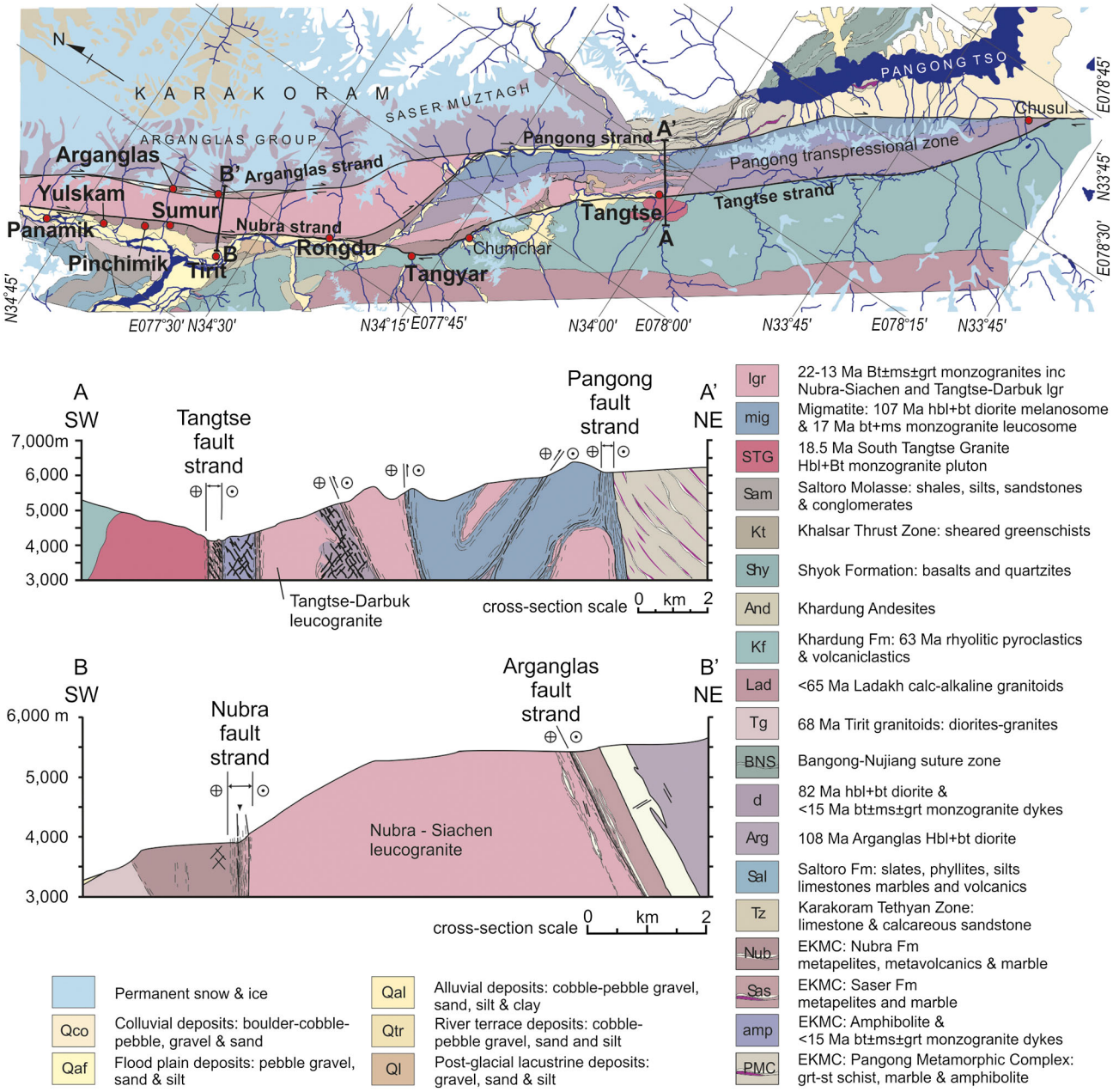

Figure 2. Central portion of the KFZ, Ladakh, N. India (modified from *Phillips* [2008]; *Phillips et al.* [2004] and *Phillips and Searle* [2007]). Cross section A-A′ shows the Tangtse and Pangong fault strands near Tangtse. Cross section B-B′ shows the Nubra and Arganglas fault strands in Tirit gorge. Sample localities are marked: **Pinchimik** - MLA1B, W11/1; **Panamik** - P72a, P72b-3; **Yulskam** - P77, P78, P80, P82, P83, P85, P86, P87/1-2, P88, P89/1, P89/2, W11/7; **Sumur** - W11/20, W11/29, and W11/41; **Arganglas** - P144, P145, P146, P149, P150, W11/49, W11/52, W11/56; **Rongdu** - P152, P155, P156; **Tangyar** - P185, P187, P189; **Tangtse** - P1, P4, P10, W11/66, W11/102, W11/109.

rocks formed at depth within the crust. If a fault continued to be active during exhumation, a sequence of progressively lower temperature overprinting fault rocks may form, providing information on deformation over a wide range of depths.

[8] Of particular interest are deformation processes and weakening mechanisms that operate in the transitional zone between the brittle upper crust and ductile mid-lower crust. This is typically the strongest portion of the upper crust and hence the region where the effects of weakening processes can be most pronounced [e.g., *Holdsworth*, 2004]. In the shallower brittle regime, deformation occurs predominantly by fracturing, dilatancy, and frictional sliding/flow [*Scholz*, 1998]. At greater depths, increased temperature results in viscous flow dominated by intracrystalline plasticity and diffusional deformation processes [*Bürgmann and Dresen*, 2008]. The intervening zone is considered to be a complex region where lithological and structural factors [*Stewart et al.*, 2000], synkinematic metamorphism [*Brodie and Rutter*, 1985], changes in grain size [*White et al.*, 1980], the mechanical and chemical effects of pore fluids [*Tullis and*

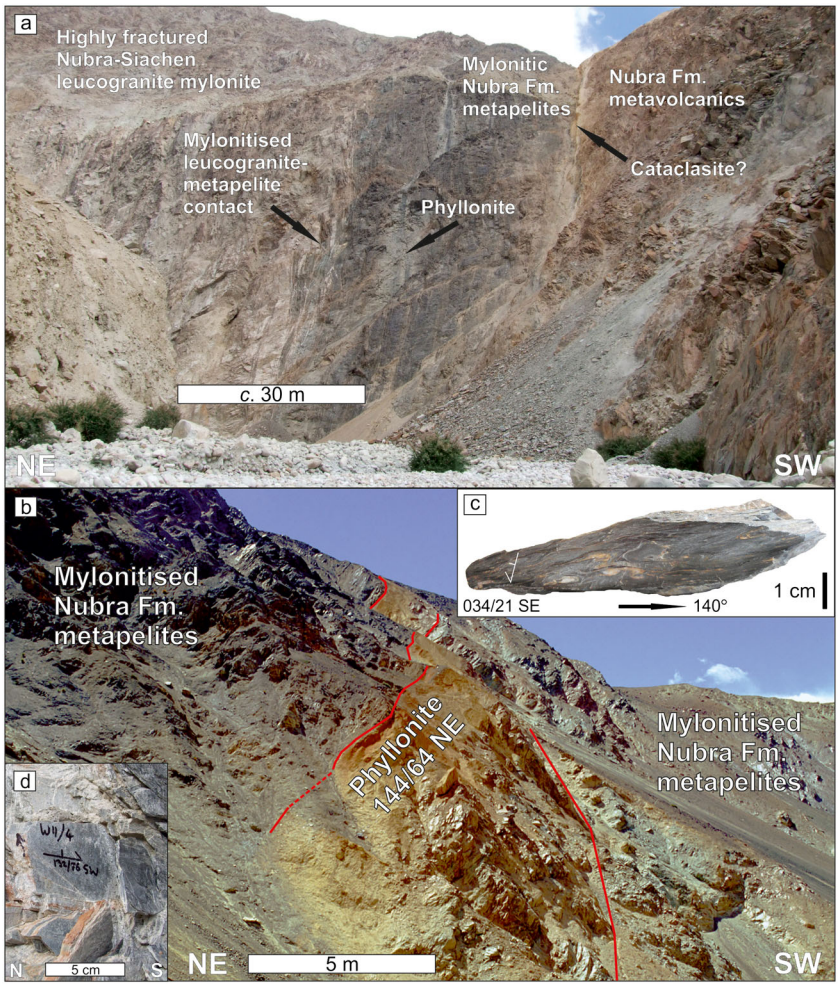

Figure 3. (a) Cliff cross section through the Nubra fault strand in Yulskam gorge. Mylonitized leucogranite and metapelites are overprinted by phyllonite, cataclasite, and distributed fracturing. (b) Phyllonite band (~10 m thick) within mylonitized metapelites of the Nubra Formation near Yulskam. Strike of phyllonite foliation (144/64NE) is subparallel to the regional-scale orientation of the Nubra fault strand (138/85NE). (c) Polished XZ surface of phyllonite from Yulskam. Coarser-grained phyllosilicate bands (black) form interconnected layers through fine-grained matrix of phyllosilicates and framework silicates (dark grey) and deformed quartz veins (light grey) (Sample W11/2). (d) Mylonitized metapelites of the Nubra Formation near Yulskam. Foliation (marked) is oriented subparallel to the regional-scale orientation of the Nubra fault strand (Sample W11/4).

Yund, 1980], along with strain rate, pressure, and temperature [*Hirth and Tullis*, 1994] may all control deformation. This frictional-viscous transition zone (FVTZ) generally occurs at depths of *c*. 10–15 km [*Stewart et al*., 2000]. However, processes such as fluid influx, grain size refinement, metamorphic reactions, and changes in geothermal gradient may contribute also to its spatial evolution over time (e.g., shallowing, sometimes to as little as 5 km depth, *Imber et al*. [2001]).

[9] In this contribution, we present field and microstructural evidence for a range of fundamental fault weakening processes including the effects of pore fluids, reaction softening, and interconnected weak layer development in fault rocks exhumed from the frictional-viscous transition zone within the KFZ, NW Himalaya. The impact of these fault weakening mechanisms is considered in terms of seismicity on the fault and the character of continental lithospheric deformation.

2. Geological Setting

[10] The KFZ is a >800 km long dextral strike-slip fault that delineates the western margin of the Tibetan plateau, striking from the Mt. Kailas region of SW Tibet to the Pamirs in the NW Himalaya (Figure 1). The central portion of the KFZ in Ladakh, NW India, consists of subparallel strands linked by a transpressional left-hand jog (Figure 2). The macroscopic geometry of the fault zone in this region has been extensively mapped by *Phillips* [2008]. In this region, the KFZ juxtaposes midcrustal igneous and metasedimentary units of the southern Asian continental margin to the NE with intrusive and extrusive magmatic units of the Ladakh arc terrane to the SW [*Kirstein et al*., 2009; *Phillips*, 2008]. The Asian metasedimentary units include the Nubra Formation, Saser Formation, Pangong Metamorphic Complex (PMC), and Pangong Transpressional Zone (PTZ), collectively termed

the Eastern Karakoram metamorphic complex (EKMC). *Thakur et al*. [1981] have suggested that the protoliths of the Nubra Formation are Permian in age based on fossil fauna from limestones. The EKMC underwent polyphase mid-upper amphibolite grade metamorphism prior to the initiation of the KFZ [*Streule et al*., 2009]. The Nubra and Arganglas fault strands in the north of the area link with the Tangtse and Pangong strands, respectively, in the south, where they are intersected by the linking jog (Figure 2). Transpression on this jog has resulted in exhumation of the PTZ, a deep upper-amphibolite grade migmatite terrane between the Tangtse and Pangong fault strands [*Searle and Phillips*, 2007]. Detailed outcrop scale descriptions of deformation on the Tangtse and Pangong fault strands are provided by *Rutter et al*. [2007]. Ductile deformation microstructures (e.g., undulose extinction and bulging grain boundaries in feldspars and subgrains and interlobate grain boundaries in quartz) are well developed in granitoid rocks on each fault strand [*Phillips and Searle*, 2007]. Assuming a strain rate of the order of 10^{-13} s^{-1} (i.e., 120 km offset accumulated within two homogenously deforming 1 km wide shear zones over 15 Ma, see below), these microstructures indicate that deformation at the exposed structural level occurred in the solid state at temperatures spanning *c*. 400–550°C [*Stipp et al*., 2002]. Asymmetric deformation microstructures, such as mantled porphyroclasts and S-C fabrics, indicate dextral deformation on each fault strand. Brittle deformation has previously been considered to be limited to the Nubra and Pangong fault strands, being transferred from one to the other by the linking jog [*Rutter et al*., 2007].

[11] The Nubra fault strand (Figures 2 and 3a) is located at the contact between the 15.9 Ma Nubra-Siachen leucogranite batholith and the metavolcanic and metapelitic lithologies of the Nubra Formation [*Phillips et al*., 2004]. Ductile deformation fabrics are widespread in both the leucogranite and Nubra Formation with strain grading toward a maximum intensity at the lithological contact. A *c*.10 m wide band of highly strained phyllonite that cuts through the Nubra Formation metapelites is considered to be the result of more localized deformation within the FVTZ (Figure 3). Brittle deformation is again localized at the margin of the leucogranite batholith and consists of a 4 m wide zone of intensely cataclased rock. More distributed brittle fractures are present for >2 km into the batholith [*Phillips and Searle*, 2007].

[12] The Arganglas fault strand is located at the NE margin of the Nubra-Siachen leucogranite (Figure 2). Here a <1 km wide, 35 km long band of marbles and metapelites of the Saser Formation is bounded by the Nubra-Siachen leucogranite to the SW and the 107.2 Ma Arganglas diorite to the NE [*Phillips et al*., 2013; *Phillips and Searle*, 2007]. Deformation is focused within the weaker Saser Formation, with the Arganglas diorite undeformed at distances of a few hundred meters from the fault strand. Mineral and stretching lineations within the Nubra and Arganglas strands are subhorizontal [*Phillips and Searle*, 2007].

[13] The Tangtse fault strand in the Tangtse valley (Figure 2) consists of 120 m width of highly deformed marbles, calc-silicates, and metapelites of the EKMC, bounded by the 15.6 Ma Tangtse-Darbuk leucogranite to the NE and the 18.5 Ma hornblende-biotite-bearing South Tangtse granite to the SW [*Phillips et al*., 2004; *Leloup et al*., 2011]. The Tangtse fault strand forms the SW margin of the PTZ. The NE margin is formed by the Pangong fault strand, which juxtaposes deeply exhumed migmatitic metapelites, granodiorite, and leucogranite of the PTZ against slightly lower grade metasediments of the PMC. Lineations in both the Tangtse and Pangong fault strands plunge *c*. 20° NW as a result of transpressional exhumation of the PTZ [*Rutter et al*., 2007].

[14] Each of the Nubra, Arganglas, and Tangtse fault strands is located along bands of the EKMC (Nubra Fm., Saser Fm., and PTZ, respectively) situated between various granitoids. Within each fault strand, the most intense deformation fabrics are located at the contacts between metasedimentary and granitoid lithologies [*Phillips and Searle*, 2007]. These observations provide a first-order indication of weakness of the metasedimentary lithologies (primarily metapelites and marbles) relative to the granitoids and suggest that the deformed metasedimentary and granitic rocks have a significant rheological contrast with the undeformed granitoids.

[15] The age, offset, depth of penetration, and geological slip rate on the KFZ are the subject of considerable debate (see *Searle et al*. [2011] for a review). Offsets of geological markers [*Murphy et al*., 2000; *Wang et al*., 2012, 2013; *Zhang et al*., 2011] including the Baltoro-Nubra leucogranite batholith [*Phillips et al*., 2004, 2013; *Searle and Phillips*, 2007; *Searle et al*., 1998], the Shyok suture zone [*Phillips et al*., 2004], the Triassic-Jurassic Aghil formation [*Robinson*, 2009], and the antecedent Indus river [*Gaudemer et al*., 1989; *Searle*, 1996; *Valli et al*., 2007] are in the range 40–150 km. Offsets of 250–565 km have also been proposed for differing interpretations of the same structures [*Lacassin et al*., 2004a; *Valli et al*., 2008]. *Klemperer et al*. [2013] present helium isotope ratios which they suggest show that the KFZ penetrates to the mantle. However, cross sections based on the regional structure of the NW Himalaya-Karakoram show the KFZ as an upper-midcrustal structure only [*Searle et al*., 2010, 2011]. *Phillips et al*. [2004] provided robust constraints on the age of the Nubra and Tangtse strands of the fault based on U-Pb isotope dilution thermal ionization mass spectrometry data from prekinematic and postkinematic leucogranites, inferring that ductile deformation at the currently exposed structural level initiated between 15.68 ± 0.5 Ma and 13.73 ± 0.3 Ma. These ages concur with initiation ages of 14–12 Ma along the southern portion of the KFZ [*Murphy et al*., 2000; *Wang et al*., 2012].

[16] Published slip rates for the KFZ vary widely. The most reliable slip-rate estimates from geological [*Murphy et al*., 2000; *Phillips et al*., 2004; *Wang et al*., 2012], geomorphological [*Brown et al*., 2005; *Chevalier et al*., 2012; *Robinson*, 2009], and geodetic [*England and Molnar*, 2005; *Meade*, 2007; *Wang and Wright*, 2012; *Wright et al*., 2004] observations are typically in the range 3–10 $mmyr^{-1}$. However, within the historic and instrumental record periods, the KFZ has generated limited seismicity with no significant events recorded (Figure 1). The seismogenic potential of the KFZ, with regard to the observed deformation mechanisms, is discussed below.

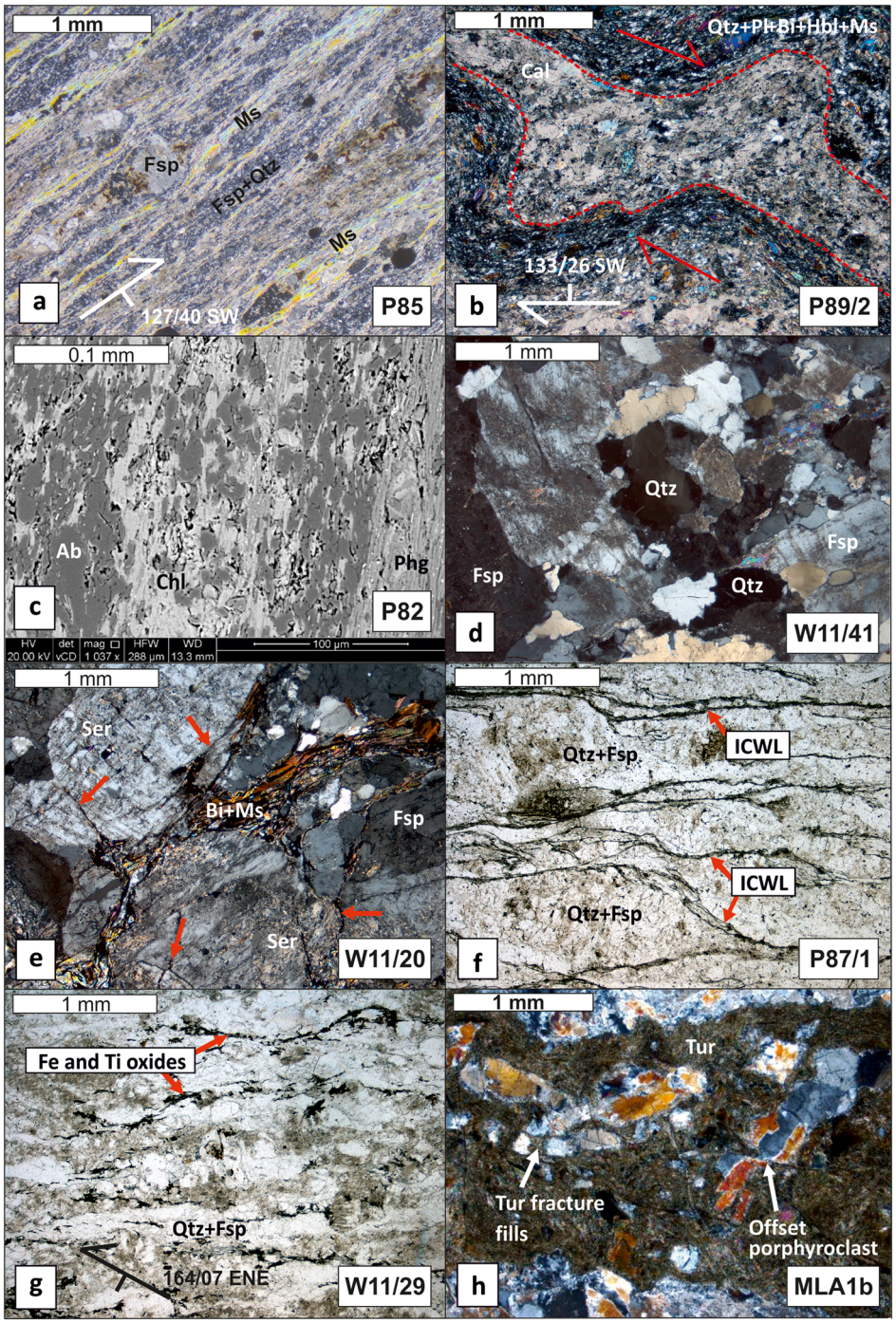

Figure 4. Deformation fabrics on the Nubra fault strand. (a–c): Nubra Formation, (d–h): Nubra-Siachen leucogranite. Figures 4a, 4b, 4d, 4e, and 4h are crossed-polar optical images, Figure 4c is SEM backscattered electron atomic number contrast, and Figures 4f and 4g are plane polarized optical images. (a) Mylonitic metapelite with through-going bands of muscovite (Ms) separating layers of fine-grained quartz (Qtz) and feldspar (Fsp). Sample P85. (b) Dextrally sheared calcite vein in mylonitic andesitic metavolcanics. Sample P89/2. (c) Phyllonite with layers of phengite (Phg) and chlorite (Chl) wrapped around albite (Ab) grains. Albite grains indent one another at contacts. Sample P82. (d) Coarse-grained leucogranite from centre of Nubra-Siachen batholith. Sample W11/41. (e) Leucogranite 70 m from SW margin of batholith. Microfractures (red arrows) are associated with sericite (Ser). Biotite (Bi) and Muscovite (Ms) form layers. Sample W11/20. (f) Leucogranite from margin of batholith with interconnected weak layers (ICWL) of fine-grained biotite and muscovite porphyroblasts. Sample P87/1. (g) Leucogranite from margin of batholith with abundant Fe and Ti oxides along sericitic layers (brown). Sample W11/29. h) Breccia and cataclasite generated from leucogranite protolith and entrained within infiltrating green-brown ultrafine-grained tourmaline (Tur) veins. Fractures are mostly extensional (left) but some show dextral offset (right). Sample MLA1B.

3. Deformation Mechanisms Within the KFZ

3.1. Deformation on the Nubra Fault Strand

3.1.1. Deformation Microstructures Within the Nubra Formation

[17] On the Nubra fault strand, metapelites of the Nubra Fm. show mylonitic-ultramylonitic tectonic fabrics (Figure 4a, samples P85, P86, P156, and W11/7). These contain varying proportions of Qtz + Fsp + Ms + Bt ± Grt ± Ky ± Chl ± Cal. Quartz invariably shows almost complete grain size reduction to <50 μm. Within monominerallic polycrystalline quartz aggregates, grain boundaries are rounded-interlobate whereas the boundaries of isolated grains (typically bounded by micas) are rounded-straight.Quartz subgrains (20–30 μm) are extensively developed. Feldspar porphyroclasts in W11/7 are fractured, elongated, and ~50% altered to sericite. Foliation within the metapelites is defined by alignment of muscovite, biotite, and kyanite. The micas form either through-going subparallel bands (W11/7) or dextral S-C′ fabrics (P85). These constitute up to 35% of the minerals visible in the plane of section (i.e., parallel to lineation and perpendicular to foliation; the XZ plane of finite strain). Micas show undulose extinction with split and stacked cleavage planes and bent grains. Muscovite is typically coarser than biotite and forms fish structures.

[18] Metavolcanics of the Nubra Fm. show protomylonitic-mylonitic tectonic fabrics. The metavolcanic mineralogies indicate andesitic (varying proportions of Pl + Kfs + Ep + Qtz + Ms + Chl + Hbl + Cal, samples P77, P78, and P89/2) or basaltic (Pl + Cpx + Opx + glass, sample P80) protoliths. In the andesitic samples, quartz has undergone extensive grain size reduction. The few remaining porphyroclasts (~300 μm) are generally rounded with undulose extinction, whereas ~35 μm matrix grains typically have lobate grain boundaries and contain numerous subgrains. Feldspars show either partial or complete reduction in grain size. Feldspar porphyroclasts (150–700 μm) show bulging boundaries whereas finer matrix grains are typically rounded. Feldspar in sample P78 is almost completely sericitized. Epidote and hornblende are found as isolated grains, approximately 160 μm and 600 μm, respectively. Hornblende grains commonly have straight grain boundaries. Foliation is defined by porphyroclast and matrix grain alignment and alignment of subparallel ~100 μm wide fine-grained sericitic shear bands. P78 shows a strong dextral S-C fabric. The basaltic protomylonite contains subhedral-euhedral 150–900 μm phenocrysts of orthopyroxene and clinopyroxene in a glassy groundmass with microlitic plagioclase. Foliation is defined by phenocryst and <40 μm matrix grain alignment but the tectonite fabric is weaker than in the andesitic specimens.

[19] Both the metavolcanics (P89/2) and metapelites (sample P86) of the Nubra Formation contain monominerallic layers of either calcite (P89/2) or quartz (P86). In P89/2, <650 μm thick folded calcite layers are parallel to the folded cleavage of the andesitic metavolcanic (Figure 4b). The layers have sharp contacts with the metavolcanic host material. Individual ~50 μm grains have highly irregular bulging boundaries and contain numerous 20–30 μm subgrains. In P86, 200–300 μm quartz layers are parallel to the straight cleavage of the metapelite and again have sharp contacts. Unlike the folded calcite veins, quartz veins show occasional boudinage. The <70 μm quartz within these layers has aspect ratios of ~2:1 with a shape preferred orientation aligned 25° to the foliation and layer margins. Rounded quartz subgrains (~30 μm) are ubiquitous within these layers.

[20] Marbles are found locally within the Nubra Fm. at Rongdu (samples P152 and P155, Figure 2). These are composed of calcite with minor isolated grains of quartz and muscovite. Calcite consists of 250–300 μm porphyroclasts with bulging grain boundaries and mantles of 30–40 μm irregular-shaped grains. Porphyroclasts contain <30 μm wide curved and wavy twins (i.e., type III of *Burkhard* [1993]).

3.1.2. Deformation Microstructures Within Nubra Formation Phyllonites

[21] The metavolcanics and metapelites are cut by a <10 m wide phyllonite band (Figure 3) showing a (Pl + Qtz + Chl + Phg) greenschist facies assemblage (samples P82, P83, and W11/1), with abundant sericitic layers and foliation parallel layers of pure calcite visible in outcrop. In coarser-grained phyllonite at Yulskam (sample W11/1, Figure 2), 250–400 μm thick porphyroclastic quartzo-feldspathic domains are separated by much finer-grained 150–200 μm thick bands rich in sericite (50–100%). These bands define a well-developed S-C′ fabric. Quartz porphyroclasts (~250 μm) show strong undulose extinction, occasional 40 μm marginal subgrains, and bulging grain boundaries. Matrix quartz (<20 μm) has irregular-shaped boundaries and aspect ratios <3:1. Feldspar porphyroclasts (~300 μm) are rounded and highly sericitized. In finer-grained phyllonites at Rongdu (Samples P82 and P83, Figure 2), S-C′ fabrics are locally preserved in thin section but the microstructure is dominated by subparallel and anastomosing 100–300 μm thick layers of chlorite and phegitic white mica which are interlayered with 40–200 μm thick quartzo-feldspathic domains and define the foliation. Layer composition varies between pure phyllosilicates, pure framework silicates, and mixtures of the two. In backscattered electron images (Figure 4c), chlorite and phengite are present as interconnected layers that wrap around aligned ~10 × 20 μm grains of albite. Albite generally exhibits straight grain boundaries forming the sides running parallel to foliation, but sutured and indented boundaries where the ends of albite grains come in contact along sides running normal to foliation. The phyllonites at both localities generally lack microscopic evidence of brittle deformation (e.g., fractures or relict fragments of cataclasite).

3.1.3. Deformation Microstructures Within the Nubra-Siachen Leucogranite

[22] The NE margin of the Nubra fault strand consists of garnet 2-mica leucogranite (Qtz + Ksf + Pl + Bt + Ms + Grt) and K-feldspar megacrystic monzogranite (Qtz + Ksp + Pl + Bt ± Ms) of the Nubra-Siachen leucogranite batholith. Furthest from the Nubra and Arganglas fault strands (i.e., near the center of the batholith, Figure 4d, sample W11/41, 1890 m NE of the Nubra strand), these granites contain *c*. 1 mm grained feldspars with numerous feldspar-feldspar contacts, euhedral-subhedral morphologies, and well-preserved igneous zoning. Feldspars have been altered by 0–50% to patchy sericite. Rare transgranular fractures crosscut each mineral and show no particular spatial relationship to sericite. Quartz is typically coarse grained (250–500 μm) with lobate grain boundaries and patchy undulose extinction. Primary micas (<5%) are coarse grained (<0.5 mm), have weak undulose extinction, show a weak grain shape preferred orientation, and are isolated amongst quartz and feldspar.

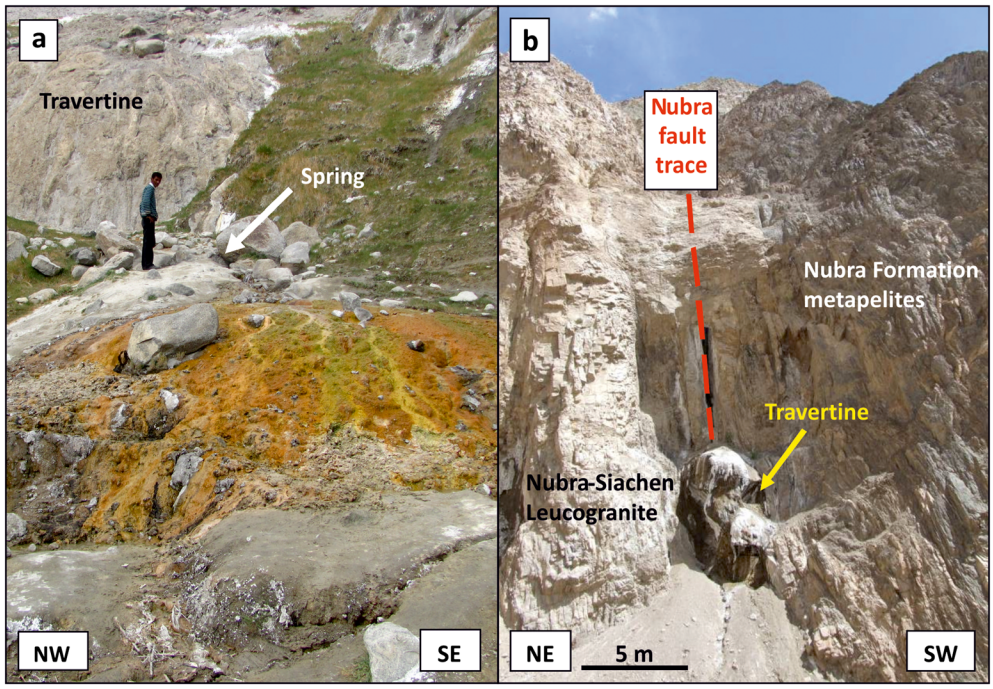

Figure 5. Evidence of hydrothermal activity on the Nubra fault strand. (a) Active hydrothermal springs and travertine deposits on the fault trace at Panamik. (b) Travertine deposits within the fault core at Sumur indicate palaeohydrothermal activity.

[23] In samples closer to the margin of the batholith and within the Nubra fault strand (W11/20, 70 m NE of the batholith margin and samples P72a, P87/1, P87/2, P88, and P89/1), feldspars are still coarse grained (<10 mm) but intercrystalline microfractures are abundant within them. These microfractures are spatially associated with an increased proportion of sericite, which has replaced 50–100% of the area of the feldspar grains (Figure 4e). Mixtures of aligned biotite (<300 μm) and sericite are found as through-going bands *c*. 100–300 μm thick that anastomose and wrap around feldspar grains, closely following feldspar grain boundaries. These bands form an irregular but semicontinuous network throughout the rock mass. Feldspars show intragranular crystal plastic deformation microstructures such as bent and tapered deformation twinning and patchy undulose extinction, along with bulging grain boundaries and thin (*c*. 100 μm) mantles of fine-grained neoblasts. Quartz is considerably finer grained (50–500 μm) than in the center of the batholith. Its grains have highly irregular interlobate boundaries, ubiquitous 50 μm rounded subgrains and neoblasts and are locally highly flattened (axial ratios >5:1) where they appear "squeezed" between feldspar grains. Individual *c*. 300 μm grains of calcite are occasionally present.

[24] In leucogranite from the very SW margin of the batholith and within the center of the Nubra fault strand (sample W11/29), feldspar grain size is considerably reduced (<500 μm) and fine-grained matrix neoblasts of feldspar are abundant and intermixed with quartz. However, sericite has almost completely replaced (>80%) original feldspar such that it constitutes <40% of the rock. Sericite patches and bands are therefore highly interconnected forming a foliation parallel network (Figure 4f). Where preserved, crystal plastic deformation microstructures in feldspar are similar to those in sample W11/20, as are those in quartz. Sample W11/29 shows abundant strings of opaque Fe- and Ti-oxide grains along the fine-grained micaceous foliae (Figure 4g). Here the opaques are considerably more abundant than in samples with less intense tectonic fabrics or in portions of the sample lacking in mica foliae. This sample also contains 1–2 mm thick foliation parallel quartz veins. Quartz within the veins shows lobate/cuspate grain boundaries and abundant subgrains, identical to quartz microstructures in the host leucogranite.

3.1.4. Tourmaline ± Quartz Veins on the Nubra Fault Strand

[25] Ultrafine-grained tourmaline ± quartz veins <1 mm up to a few cm thick are emplaced within the Nubra-Siachen leucogranite along the Nubra fault strand (Figure 4h). These were originally identified as pseudotachylytes based on field observations [*Phillips and Searle*, 2007]. However, scanning electron microscope and electron microprobe analyses have subsequently been used to determine their tourmaline-rich mineralogy [*Phillips*, 2008; *Watkins*, 2011]. The veins infill brittle fractures that crosscut ductile deformation fabrics in the leucogranites and monzogranites. The veins strike 050–070° approximately perpendicular to the strike of the KFZ [*Watkins*, 2011]. The tourmaline veins commonly include numerous fragments of fractured host mylonitic leucogranite. Occasionally, shear offsets of host rock grains across the veins are visible in thin section. More commonly, host rock fragment geometries suggest vein normal extensional opening.

3.1.5. Hydrothermal Springs Along the Nubra Fault Strand

[26] Hydrothermal springs emerge along the fault trace around Panamik village (Figure 5a). The hydrothermal fluids emerge at 28–76°C and contain 2–8 mg/kg of boron [*Absar et al*., 1991]. The active springs at Panamik are immediately adjacent to travertine deposits. Similar travertines are found precipitated onto the exhumed core of the Nubra fault strand

in Sumur gorge within a *c*. 2 m wide zone of cataclasite along the margin of the Nubra-Siachen leucogranite (Figure 5b). It is clear from field relations that the travertine in Sumur gorge postdates the foliated mylonites and cataclasites onto which it is deposited but also that hydrothermal fluids must recently have flowed through the fault to the surface at this locality. Other active hydrothermal springs also occur on the trace of the KFZ in the Nubra valley at Changlung and Pulithang, 15 km NW and 5 km SE from Panamik, respectively [*Absar et al*., 1991].

3.2. Interpretation of Deformation Mechanisms Within the Nubra Fault Strand

[27] In order to estimate the depth of operation of particular deformation processes, we estimate the temperature at which they operated and assume typical geological shear zone strain rates of 10^{-12}–10^{-14} s^{-1} (a reasonable assumption in the KFZ, see above) and a typical Miocene Karakoram geothermal gradient of 30°Ckm^{-1}. This thermal state prevailed across much of the wider Baltoro Karakoram as a result of crustal thickening [e.g., *Palin et al*., 2012] and therefore does not suggest significant localized shear heating within the fault zone as proposed by Rolland *et al*. [2009] (*cf*. section 4.7). In order to estimate the time at which particular deformation processes operated, we compare the estimated deformation temperatures to published thermochronometric data.

[28] Quartz microstructures within both the metavolcanics and metapelites of the Nubra Formation are characteristic of deformation by grain boundary migration (GBM) and subgrain rotation (SGR) dynamic recrystallization. Feldspar microstructures are characteristic of deformation by bulging (BGL) dynamic recrystallization. These deformation mechanisms suggest that deformation occurred at temperatures of 450–550°C (15–18 km depth) [*Stipp et al*., 2002]. Split and stacked cleavage in micas indicate that they deformed by frictional slip on these planes. The presence of strong undulose extinction suggests that dislocation climb was limited and therefore that recovery dominated dynamic recrystallization was not a significant deformation mechanism for micas.

[29] Quartz and calcite veins within the Nubra Formation are recrystallized. Quartz subgrain microstructures in the veins indicate SGR deformation at 400–500°C. Larger quartz grains with lobate/cuspate boundaries indicative of GBM are absent from the veins. This suggests either that significant deformation at >500°C did not affect the veins (i.e., they were emplaced during deformation and exhumation) or that GBM microstructures have been overprinted at lower temperatures by extensive SGR. As much of the host rock preserves GBM quartz microstructures, we tentatively suggest that the veins were emplaced during deformation at 400–500°C (13–17 km depth). If this is correct, then the veins provide evidence for boron-rich pore fluids at pressures great enough to promote fracturing during vein formation at depths where deformation was otherwise dominantly ductile. Calcite microstructures in marble pods and lenses at Rongdu (Figure 2) are characteristic of BGL dynamic recrystallization at >250°C whilst type III twinning is evidence for ongoing deformation at 200–250°C (>8 km and 7–8 km, respectively) [*Burkhard*, 1993].

[30] Phyllonites within the Nubra strand consist of fine-grained intermixed and layered phyllosilicates and framework silicates. The abundant chlorite, phengite, and finer-grained sericite are well aligned in interconnected layers and would have deformed easily by slip on basal (001) planes oriented (sub)parallel to the macroscopic fault shear plane. Rare dynamic recrystallization microstructures and undulose extinction in quartz and feldspar suggest that dislocation climb was limited and therefore indicates that deformation in the phyllonites occurred at <400°C (<13 km depth). At these lower temperatures, feldspar grains would have behaved as rigid bodies. In samples P82 and P83, elongate feldspar grains can be seen to indent one another where their ends come into contact, showing the effects of removal of material by dissolution. The combination of frictional slip on phyllosilicate foliae and dissolution of rigid clasts at high stress sites suggests that the phyllonite deformed by frictional-viscous flow [*Bos and Spiers*, 2002]. The microstructure of the phyllonite bears remarkable resemblance to the microphysical model microstructure of frictional-viscous flow of *Bos and Spiers* [2002]. *Bhutani et al*. [2003] obtained an Ar-Ar age of 13.9 ± 0.1 Ma for biotite from sheared granite near Panamik. This age provides an indication of the approximate time at which the rocks of the exposed structural level on the Nubra strand cooled through the greenschist facies conditions under which phyllonitization occurred.

[31] In the center of the Nubra-Siachen leucogranite batholith, the leucogranite is essentially undeformed. Quartz shows some evidence of grain boundary migration but feldspars are undeformed and sericitization is patchy and limited to <50%. The numerous feldspar-feldspar contacts and only isolated grains of biotite and muscovite indicate that the rheology of the rock is that of a relatively rigid load-bearing framework [*Handy*, 1990]. The leucogranite has a weak primary fabric defined by poorly aligned biotite and feldspar megacrysts but lacks evidence of any significant submagmatic deformation (e.g., imbricated feldspars or late magmatic mineral growth in pressure shadows).

[32] In samples approaching the margin of the batholith and the Nubra fault strand, quartz grain shapes still indicate GBM dynamic recrystallization but increasingly reduced grain size and subgrain development indicate a significant contribution of SGR. Microstructures in unaltered feldspar indicate deformation by BGL dynamic recrystallization. As in the Nubra Formation, these quartz and feldspar deformation mechanisms indicate deformation temperatures of *c*. 500°C (*c*. 17 km depth). Interconnected bands of sericite and coarser-grained micas in samples within the fault strand are inferred to have deformed by frictional slip on their aligned basal (001) planes. The increased abundance of opaque phases adjacent to the phyllosilicate foliae indicates that they are residual from dissolution of quartz or feldspar. Grain boundary contact with mica or clay minerals is known to enhance rates of pressure solution in quartz [*Dewers and Ortoleva*, 1991; *Hickman and Evans*, 1995; *Hippertt*, 1994; *Houseknecht*, 1988]. The increased abundance of opaques at quartz/feldspar boundaries in contact with mica suggests that micas acted to enhance the rate of dissolution of the adjacent minerals. Quartz veins present in one such sample (W11/29) contain quartz microstructures indicative of combined GBM + SGR dynamic recrystallization. These veins are therefore inferred to have formed at a similar depth (i.e., similar time) to the deformation microstructures in the leucogranite. These veins provide evidence for silica-saturated fluids within the rock. This suggests that veining provided a sink for material dissolved at mica grain boundaries. These observations

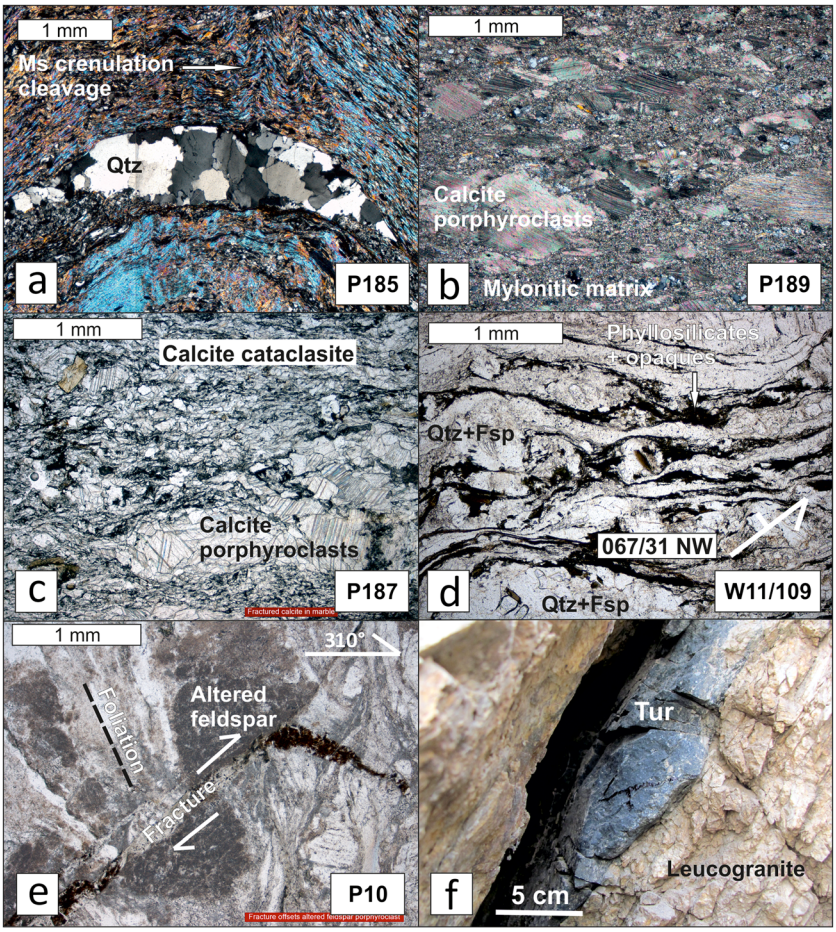

Figure 6. Deformation microstructures on the Tangtse fault strand. (a–c) EKMC, (d–f) Tangtse-Darbuk leucogranite. Figures 6a and 6b are cross-polarized optical images and Figures 6c–6e are plane polarized. (a) Folded metapelite with tapered quartz (Qtz) vein across fold hinge and M-fold muscovite crenulation cleavage. Sample P185. (b) Calc-mylonite with elongate twinned porphyroclasts in fine mylonitic matrix. Sample P189. (c) Marble cataclasite with angular fractured porphyroclasts and cataclastic matrix. Sample P187. (d) Leucogranite from SW margin of Tangtse-Darbuk leucogranite pluton. Through-going fine-grained black bands are composed of phyllosilicate and opaque minerals. These separate domains of highly deformed quartz and feldspar (Fsp). Sample W11/109. (e) Leucogranite from SW margin of Tangtse-Darbuk leucogranite pluton. Ductile foliation is crosscut by dextral shear fracture with millimetric offset. Sample P10. (f) Black foliation parallel tourmaline (Tur) vein emplaced within leucogranite.

indicate that fluid-assisted diffusive mass transfer contributed to strain accommodation in the high strain zone.

[33] Tourmaline ± quartz veins emplaced within the Nubra-Siachen leucogranite crosscut ductile deformation fabrics and are associated with pervasive fractures and host rock cataclasite. They formed therefore under temperatures of <300°C, at shallow depths of <10 km.

3.3. Deformation on the Tangtse Fault Strand

3.3.1. Deformation Microstructures Within the Tangtse Strand EKMC

[34] On the Tangtse fault strand, mylonitic fabrics are preserved within metapelites, metavolcanics, and marbles that form the EKMC country rocks to the Cretaceous and Miocene intrusions within the PTZ. Metapelites (Ms + Qtz + Cal + Fsp, sample P185) contain well-aligned 100 μm flakes of muscovite (50–70%) in highly interconnected layers that are folded into 300 μm crenulation cleavage domains and cm-scale microfolds (Figure 6a). Quartz and calcite veins are present in the hinge regions of these folds, which are up to a few mm thick at fold hinges but taper out on the fold limbs. Calcite (300–450 μm) in the veins is flattened with irregular shaped boundaries and curved and tapered type III twinning [*Burkhard*, 1993]. Quartz (*c*. 400 μm) in the veins has lobate grain boundaries, deformation lamellae, and undulose extinction. Quartz in the muscovite-rich matrix on the other hand is finer grained (50 × 100 μm) with straight grain boundaries in contact with muscovite and 30 μm subgrains. Feldspar occurs in the matrix as *c*. 50 μm rounded grains.

[35] Calc-mylonites (Cal + Act + Czo, sample P189) contain flattened calcite porphyroclasts up to 100 × 300 μm with abundant curved and tapered type III twins [*Burkhard*, 1993] and bulging grain boundaries (Figure 6b). These are supported within and between 0.5 and 1 mm thick bands of <30 μm rounded calcite grains. Foliation in the calcite is

defined by alignment of elongate porphyroclasts and grain size banding. Foliation parallel bands (2–20 mm thick) of actinolite + clinozoisite consist of straight and bent <100 μm grains aligned with the calcite foliation. Quartz occurs amongst the calcite as isolated rounded 50–100 μm grains with diffuse subgrain boundaries and undulose extinction.

[36] Brittle deformation has not previously been reported on the Tangtse fault strand but marble cataclasites crop out near Tangyar (Figure 6c, sample P187). These are nearly pure calcite marbles with minor quartz. Coarse (<250 μm) -grained domains up to 1 mm thick show granoblastic textures with thick type II twins [*Burkhard*, 1993]. These are separated by <800 μm thick zones of pervasive anastomosing fractures aligned subparallel to fracture zone margins. Calcite within the fractured zones occurs as elongate angular 30–50 μm fragments.

3.3.2. Deformation Microstructures Within the Tangtse-Darbuk Leucogranite

[37] The Tangtse-Darbuk leucogranite adjacent to the Tangtse fault strand shows similar microstructures to those in the Nubra-Siachen Leucogranite. At the NE margin of the Tangtse-Darbuk leucogranite (1420 m from the SW margin of the leucogranite, Sample W11/66), feldspar within the leucogranite is coarse grained (1–2 mm) with occasional myrmekite, poorly developed mantles of fine-grained feldspar, minor-moderate intragranular and intergranular fractures, and *c*. 40% sericite. Feldspars are frequently in grain boundary contact. Quartz aggregates are present as elongate foliation parallel ribbons, within which grains are relatively coarse (200–600 μm) with lobate grain boundaries, weak undulose extinction, and few subgrains. Primary igneous micas are present as isolated grains and the microstructures lacks interconnected layers of phyllosilicates. Opaque minerals are rare.

[38] In the margins of the Tangtse fault strand (sample W11/102, 690 m from the SW margin of the leucogranite), feldspar porphyroclasts are coarse (0.8–2 mm) but have bulging grain boundaries and well-developed mantles of fine-grained feldspar. Fracturing and sericitization (20–40%) of porphyroclasts are limited. However, sericite is abundant in the matrix in association with fine-grained matrix feldspar and forms narrow (20–100 μm thick) elongate layers with primary biotite. Whilst extensive, these layers are only partially interconnected and most do not cross an entire thin section. Phyllosilicate layers are decorated with fine-grained opaques. Quartz is flattened with highly irregular grain boundaries, numerous 40–50 μm subgrains, and strong sweeping undulose extinction.

[39] Within the Tangtse fault strand (sample W11/109, 390 m from the SW margin of the leucogranite), feldspar porphyroclasts are smaller (300–1500 μm) and the proportion of fine-grained matrix is increased. Few intragranular or intergranular fractures are present within porphyroclasts. Phyllosilicate-rich layers are extensive, well interconnected, and can be traced across the length of thin sections (Figure 6d). These layers are again associated with fine-grained opaque Fe and Ti oxides. At the SW margin of the leucogranite (Sample P10), transgranular fractures crosscut the mylonitic foliation at angles of *c*. 45° and show millimetric dextral offsets of altered feldspar porphyroclasts (Figure 6e).

[40] Further brittle deformation on the Tangtse fault strand is evident as ultrafine-grained black tourmaline veins emplaced within the Tangtse-Darbuk leucogranite, similar to those on the Nubra fault strand (Figure 6f). These range from stockworks of sub-mm veins that pervade disaggregated leucogranitic host rock to massive veins up to a few cm thick. Unlike on the Nubra strand, the tourmaline veins on the Tangtse strand strike subparallel to the ductile foliation.

3.4. Interpretation of Deformation Mechanisms Within the Tangtse Fault Strand

[41] Metapelites within the Tangtse fault strand contain abundant muscovite that deformed by folding in the hinge regions of crenulations and cm-scale folds. As muscovite makes up the majority of the rock volume and is highly interconnected, it is also likely to have deformed by frictional slip on its basal (001) planes. Subgrains within matrix quartz grains indicate SGR dynamic recrystallization but migration of grain boundaries appears to have been hindered by pinning against the abundant muscovite. This suggests 400–500°C as a minimum deformation temperature estimate [*Stipp et al*., 2002]. Quartz and calcite veins, present only in fold hinge regions, indicate that vein formation was synkinematic and that fluid pressures were high enough to induce extensional failure parallel to the minimum principle stress direction. Quartz microstructures in the veins indicate GMB dynamic recrystallization with a weak low temperature (<300°C) overprint. Consideration of matrix and vein quartz deformation microstructures suggests therefore that deformation occurred at up to *c*. 550°C (<18 km depth). Type III twins [*Burkhard*, 1993] in calcite veins suggest further deformation at 200–250°C (7–8 km depth).

[42] Calc-mylonites contain calcite deformation microstructures indicative of extensive mylonitization by BGL dynamic recrystallization, suggesting deformation temperatures of >250–300°C (8–10 km depth). Type III twinning [*Burkhard*, 1993] in calcite porphyroclasts is inferred to have formed at lower temperatures of 200–250°C (7–8 km depth). In the marble cataclasites, pervasive fracturing affected previously relatively undeformed marble at low temperatures (<200–250°C, <8 km depth).

[43] The Tangtse-Darbuk leucogranite is relatively undeformed at its NE margin, distal to the Tangtse fault strand, with its primary igneous microstructure largely preserved. Evidence of submagmatic deformation, such as imbricated grains or magmatic mineral growth in pressure shadows or fractures, is absent. Due to limited sericitization, low primary mica content, frequent feldspar-feldspar contacts, and coarse-grained quartz, this weakly deformed leucogranite is inferred to possess a load-bearing framework rheology [*Handy*, 1990].

[44] Toward the SW margin of the leucogranite and the Tangtse fault strand, both quartz and feldspar show increasing dynamic recrystallization. Deformation microstructures indicate that recrystallization was dominated by SGR + GMB mechanisms in quartz and BGL in feldspar, suggesting deformation temperatures of 450–550°C (15–18 km depth). As the volume of recrystallized feldspar increases, so does the proportion of sericite within it, such that it appears that grain size reduction promoted retrogressive sericitization. This may have been facilitated by increased intergranular fluid pathways and increased surface area available for reaction. The sericite, particularly in the through-going interconnected layers, is inferred to have deformed by frictional sliding. As in the Nubra-Siachen leucogranite, the increased abundance of opaque minerals associated with the phyllosilicate layers is interpreted as the result

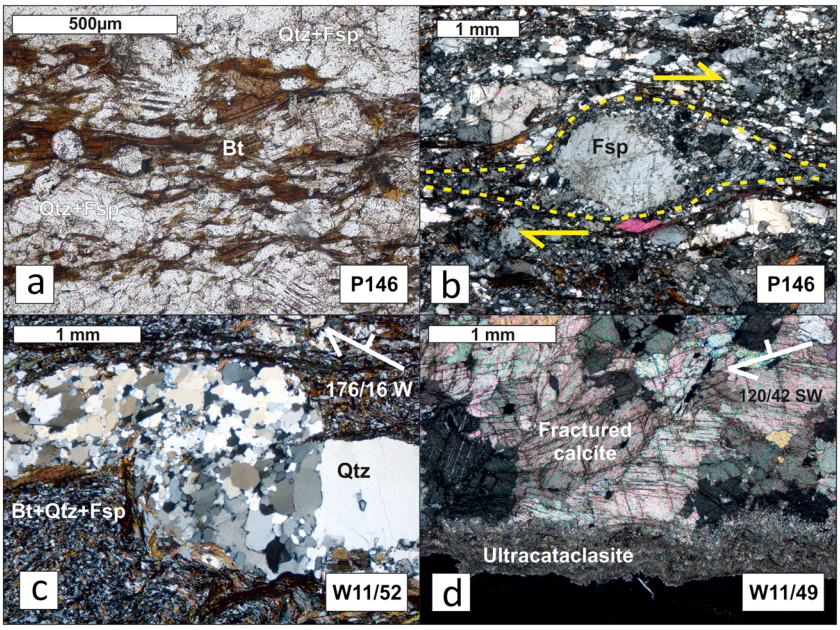

Figure 7. Deformation microstructures on the Arganglas fault strand. (a–c) Saser Formation metapelites, (d) Saser Formation marble. Figure 7a is optical plane polarized and Figures 7b–7d are cross-polarized optical images. (a) Interconnected layers of biotite (Bt) wrap around rounded porphyroclasts of quartz (Qtz) and feldspar (Fsp). Sample P146. (b) Dextral sigmoidal mantled porphyroclast of feldspar. Sample P146. (c) Dextrally folded quartz vein with coarser grained quartz in fold limb and fine-grained quartz around fold hinges. Sample W11/52. (d) Highly fractured calcite marble with ultracataclasite band. Sample W11/49.

of removal of material by dissolution during diffusive mass transfer. The extent and high interconnectivity of the phyllosilicate layers suggest that they allowed the rock to deform with an interconnected weak layer rheology [*Handy*, 1990]. The fact that water-rich fluids penetrated down to midcrustal depths at least as early as ~20 Ma is indicated by water-fluxed anatexis in the PTZ at this time [*Reichardt et al*., 2010; *Reichardt and Weinberg*, 2012; *Weinberg and Mark*, 2008] and primary CO_2- and NaCl-rich fluid inclusions in zoned plagioclase in the Tangtse-Darbuk leucogranite [*Mukherjee et al*., 2012].

[45] The ages at which sericitization occurred within both the Tangtse-Darbuk leucogranite and Nubra-Siachen leucogranite are poorly constrained. *Que and Allen* [1996] investigated sericitization of the Rosses Granite Complex, Ireland, and found that it occurred in association with fluid-induced microfracturing relatively soon after crystallization, at temperatures of 600–400°C. This may also be the case in the leucogranites of the KFZ as sericitization was coeval with development of microstructures indicating operation of grain boundary migration (>500°C) and subgrain rotation (400–500°C) of quartz and bulging dynamic recrystallization (450–600°C) of feldspar as the dominant crystal plastic deformation mechanisms. *Boutonnet et al*. [2012] modeled the thermal history of the Tangtse strand using U-Pb zircon and Ar-Ar amphibole, white mica and biotite dating, building on an earlier study by *Dunlap et al*. [1998]. Their model predicts cooling to 400°C by 12–13 Ma. *Mukherjee et al*. [2012] also obtained Ar-Ar biotite ages for the Tangtse strand from which they interpret cooling through a suggested closure temperature of 400–350°C at 10.34–9.84 Ma, ~2 Ma more recent than the model of *Boutonnet et al*. [2012]. However, if the 10.34–9.84 Ma age is instead taken to reflect cooling through a closure temperature of 320 ± 40°C [*Harrison et al*., 1985] as used by *Boutonnet et al*. [2012], then the results of both studies are in close agreement. We take therefore 12–13 Ma as the time by which sericitization of the leucogranites at the exposed structural level had occurred. Sericitization has also been found to occur at lower temperatures (e.g., 180–320°C, *Eberl et al*., 1987] through the action of heated meteoric waters. Similar retrogression may have affected the Tangtse-Darbuk leucogranite and Nubra-Siachen leucogranite as they were exhumed to shallower structural levels.

[46] Formation of the foliation parallel tourmaline veins on the Tangtse fault strand would have required extensional opening (i.e., the minimum principle stress direction) normal to the foliation. We suggest therefore that they formed after the main phase of ductile deformation on the Tangtse strand. However, they do provide evidence for high pressure fluid flow at shallower levels (<15 km depth) within this strand of the fault zone. Evidence for brittle deformation during dextral simple shear is provided by closed brittle fractures that offset porphyroclasts in the leucogranite.

[47] As on the Nubra fault strand, active hot hydrothermal springs emerge along the Tangtse strand at Chumchar and Chushul (Figure 2), although no data on the temperature or chemistry of these springs are as yet available.

3.5. Deformation on the Arganglas Fault Strand

[48] Within the Arganglas fault strand, Qtz + Bt + Fsp + Ms metapelites of the Saser formation show mylonitic fabrics (samples P146 and W11/52). Their fine-grained matrix consists of rounded feldspar and slightly elongate 40–70 µm quartz with aligned 100–300 µm biotite (30–50%). Quartz commonly contains subgrains. Biotite is distributed throughout the matrix but also concentrated in *c*. 400 µm thick subparallel layers that anastomose in

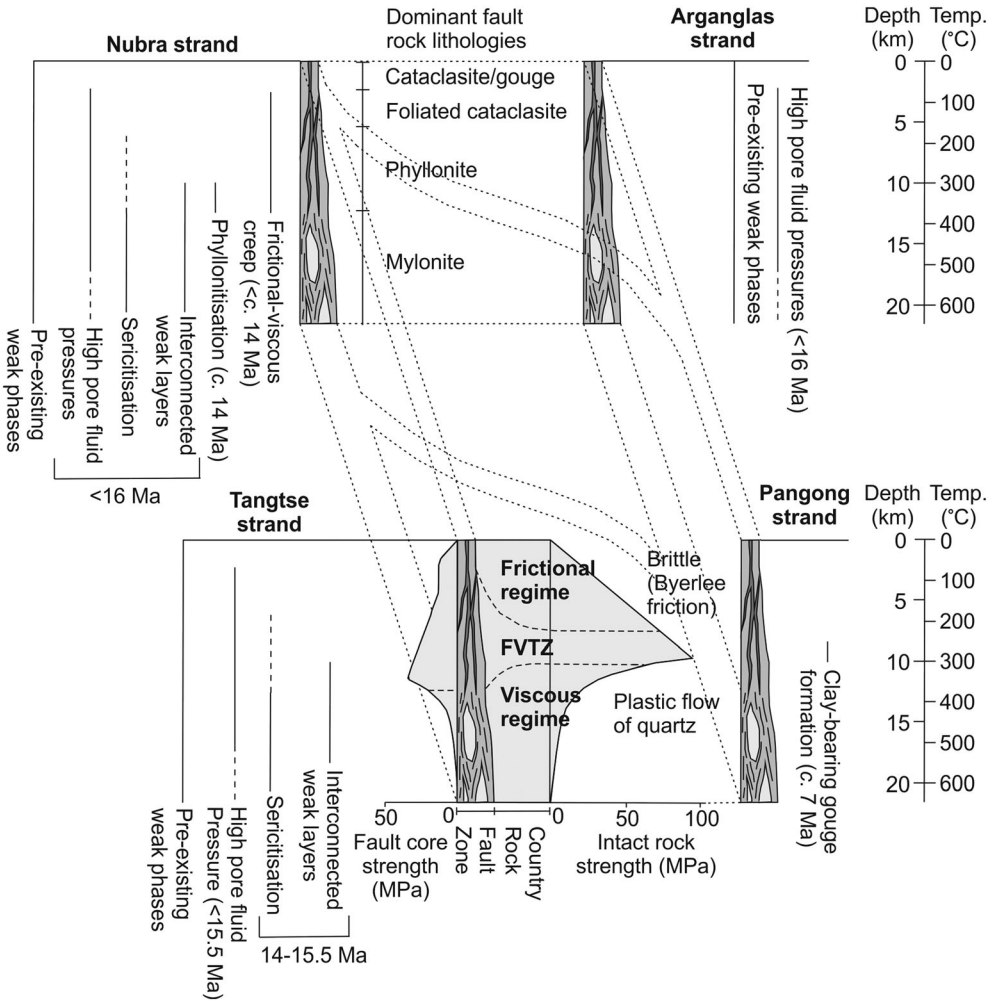

Figure 8. Schematic diagram of the KFZ showing the depths at which fault weakening mechanisms are inferred to have operated on each fault strand. Also shown are the ages at which these mechanisms began to operate, the depths typically dominated by particular fault rocks, and generalized strength-depth profiles for a weakened strike-slip fault zone and intact wall (modified from *Holdsworth* [2004]; *Imber et al*. [2008]; *Jefferies et al*. [2006a]). Temperature-depth scale assumes a geothermal gradient of 30°C/km (see main text). Inferred depth extents of fault weakening mechanisms in the KFZ inferred from metamorphic and deformation temperatures (see main text). Preexisting weak phases include biotite, muscovite, chlorite, and calcite.

dextral S-C-C′ fabrics and can be traced across entire thin sections (Figure 7a). Sample P146 contains <1.5 mm feldspar porphyroclasts with bulging grain boundaries and mantles of fine-grained rounded feldspar. These mantled porphyroclasts have strongly asymmetric dextral sigmoidal forms (Figure 7b). The same sample also contains dextral sigmoidal and rhomboidal muscovite mica fish. Sample W11/52 contains monomineralic layers of coarse-grained quartz (Figure 7c). These layers are folded with dextral vergence. Quartz in fold limbs is coarse (<700 μm) with strongly interlobate grain boundaries, sweeping undulose extinction and deformation lamellae. Within fold hinge regions, quartz is finer grained (70–100 μm) and contains numerous subgrains. An isolated metapelitic pod within marble (sample P145) consists of a coarse-grained Bt + Fsp + Tr + Cal mineral assemblage with an isotropic granoblastic texture. Constituent minerals show undulose extinction but lack other deformation microstructures. Fracturing is absent from all metapelitic samples.

[49] Marbles of the Saser formation typically consist of *c*. 90% calcite, 10% dolomite. Calcite is coarse (*c*. 800 μm) with somewhat lobate grain boundaries and abundant type II [*Burkhard*, 1993] twinning (samples P144, P149, and W11/56). Sample W11/56 is cut by bands where calcite porphyroclasts have occasional finer (100–150 μm) rounded grains at grain boundaries. Sample P150 has 150–200 μm elongate grains (axial ratio *c*. 3:1) with straight or gently curved grain boundaries, weak undulose extinction, and type II twinning. Sample W11/49 is mostly coarse grained (*c*. 700 μm) but grains are highly dissected by numerous intergranular fractures (Figure 7d). This sample contains an ultrafine-grained zone of calcite cataclasite. In the field, broad zones of blocky breccia occur at the margins of the marble bands and more intense deformation is evident in cm-scale cataclasite filled faults that cut the marble mylonites at high angles.

3.6. Interpretation of Deformation Mechanisms Within the Arganglas Fault Strand

[50] Metapelites within the Arganglas fault strand contain quartz and feldspar deformation microstructures that indicate that these minerals deformed by dynamic recrystallization dominated by SGR + GMB and BGL mechanisms, respectively. These mechanisms suggest that deformation occurred at 450–550°C (15–18 km depth). We infer that the layers of biotite within these rocks deformed by frictional slip on their aligned (001) planes. Dextral S-C-C′ fabrics, sigmoidal mantled porphyroclasts, and mica fish are consistent with previous reports of dextral strike-slip motion on this fault strand [*Phillips and Searle*, 2007].

[51] We interpret the monomineralic quartz layers in sample W11/52 as quartz veins on the basis of their coarse grain size and absence of other minerals. Interlobate grain boundaries and subgrains within the veins indicate deformation by GBM and SGR, respectively, at *c*. 500°C, consistent with deformation in the host metapelite. These veins formed therefore either before or during deformation. On the basis of comparison with similar veins within the Nubra fault strand, we tentatively suggest that these veins may be the result of elevated pore fluid pressures and fluid-assisted diffusive mass transfer during motion of the Arganglas fault strand.

[52] The majority of marbles from the Saser formation (samples P144, P149 and W11/56) show coarse, somewhat lobate grains that indicate limited deformation by GBM. Finer grains along grain boundaries in sample W11/56 may be the result of limited SGR or BGL dynamic recrystallization affecting narrow bands of the unit. The microstructure of one sample (P150) suggests the operation of grain boundary area reduction effects during static recrystallization. The variety of microstructures preserved in the marbles suggests that ductile deformation was heterogeneously distributed within them, in contrast to the ubiquitous mylonitization of the metapelites. Marble cataclasites observed in outcrop and thin section (sample W11/49), along with brecciation at the margins of marble bands, show that brittle deformation was widespread within the marbles. Fractures overprint crystal plastic deformation microstructures in the marbles and we infer therefore that it occurred subsequently at lower temperatures (<250°C) and shallower depths (<8 km).

4. Discussion: Fault Weakening Mechanisms and Their Tectonic Significance

[53] Along each fault strand of the KFZ, deformation is localized along bands of metavolcano-sedimentary lithologies and their contacts with adjacent granitoids. This indicates the relative weakness of the metavolcano-sedimentary units. In addition, several deformation mechanisms inferred to have operated within the FVTZ on each fault strand have the potential to have been weak in an absolute sense, as detailed below (Figure 8). As the prerequisites of these weakening mechanisms are still present at depth within the fault zone (i.e., the fault is likely to be deforming similar protoliths at depth to those exposed at the surface and fluid flux is ongoing), the weakening mechanisms inferred from surface exposures may be analogous to processes currently operating at depth.

4.1. Weakening Mechanisms on the Nubra Fault Strand

[54] The bulk of the Nubra Formation records ductile deformation at upper greenschist-lower amphibolite grade (450–550°C, 15–18 km depth). At these conditions, quartz and feldspar deformed by dynamic recrystallization whereas micas deformed by frictional slip on their cleavage planes. Both muscovite and biotite have been experimentally demonstrated to be frictionally weak with $\mu = 0.35–0.43$ for muscovite and $\mu = 0.25–0.40$ for biotite [*Ikari et al*., 2011; *Scruggs and Tullis*, 1998]. Their low frictional strength and abundance in the metapelites (<35%) likely resulted in a low long-term shear strength of the bulk rock (Figure 8). These preexisting weak lithologies within the Nubra (and also Tangtse and Arganglas strands) strand were present at the time at which the KFZ initiated.

[55] The main phase of ductile deformation in the Nubra-Siachen leucogranite also occurred at depths of 15–18 km. The association between microfractures and sericitization of feldspars in the deformed leucogranite suggests that fracturing facilitated fluid flow and thus promoted retrogression. Sericitization of load-bearing feldspars resulted in reaction softening and development of interconnected weak layers of phyllosilicates that deformed by frictional slip ($\mu \approx 0.4$) on cleavage planes (Figure 8). Once these weak layers formed a through-going network, they dramatically reduced the strength of the bulk rock [*Handy*, 1990; *Handy et al*., 1999; *Tullis et al*., 1991]. In addition, the formation of these phyllosilicate foliae increased the area of phyllosilicate-framework silicate grain boundary contact. This appears to have promoted dissolution of material at the contacts, allowing fluid-assisted diffusive mass transfer. Material removed in solution was redeposited as quartz veins. The veins provide evidence for pore fluids at these depths that, at least intermittently, were at pressures sufficient to promote hydrofracturing of the rock. The pore fluid pressure would have reduced the effective normal stress allowing failure at lower shear stresses than in dry rock (Figure 8). The presence of these fluids would also likely have reduced the strength of quartz during dynamic recrystallization through hydrolytic weakening [*Blacic and Christie*, 1984]. This phase of deformation is constrained by prekinematic and postkinematic leucogranites to between 15.9 and 13.7 Ma [*Phillips et al*., 2004]. Weakening processes in the leucogranites therefore began to operate in the Nubra strand <2 Ma after the initiation of faulting.

[56] Quartz veins within the Nubra Formation formed under upper greenschist conditions (400–500°C, 13–17 km depth). Their presence shows that elevated pore fluid pressures acted to weaken the rock at these slightly shallower depths (Figure 8).

[57] Phyllonitization affected the metapelites of the Nubra Formation under lower greenschist conditions (<400°C, <13 km depth) at *c*. 14 Ma. The resulting phyllonite shows microstructures suggestive of frictional-viscous flow (Figure 4c). This has been modeled to proceed with an apparent friction coefficient of 0.25–0.35 [*Bos and Spiers*, 2002]. The localized retrograde formation of phyllonites, within a *c*. 10 m wide zone, suggests that the fault zone allowed fluid influx into crust that was otherwise fluid under-saturated at this depth and time. Once formed, this mineral assemblage would have had potential to deform with less than Byerlee friction whilst being exhumed to depths of only a few km [*Bos and Spiers*, 2002] (Figure 8). Tourmaline ± quartz veins

formed within the leucogranite at depths of <10 km and provide evidence for low shear stress hydrofracturing at these shallow depths. This suggests that contrasting weakening mechanisms operated at similar depths in the phyllonites (frictional-viscous flow) and the leucogranite (hydrofracturing) within the shallow crust.

4.2. Weakening Mechanisms on the Tangtse Fault Strand

[58] Metapelites of the EKMC within the Tangtse fault strand contain a high proportion of muscovite (<70%). Low friction slip on muscovite foliation planes ($\mu \approx 0.4$) would therefore have dominated deformation of the rock. Further, quartz and calcite veins in fold hinge regions show that pore fluid pressures were sufficiently high during deformation to produce an extensional minimum principle stress. Shear stresses during deformation must therefore have been low. Quartz deformation microstructures suggest that this deformation occurred at 400–550°C (14–18 km depth) (Figure 8).

[59] Operative weakening mechanisms within the Tangtse-Darbuk leucogranite at these depths were similar to those in the Nubra-Siachen leucogranite. However, in the Tangtse-Darbuk leucogranite, sericitization appears to scale more closely with increasing recrystallization of feldspar, rather than microfracturing. We suggest therefore that grain size reduction during recrystallization increased both intergranular pathways for fluids and surface area available for reaction. The ensuing sericitization resulted in significant reaction softening of the rock and the development of through-going weak phyllosilicate layers (Figure 8). Increased opaque minerals along these layers again suggest that the phyllosilicates promoted fluid-assisted diffusive mass transfer during deformation at 15.6–13.7 Ma for the exposed structural level [*Phillips et al*., 2004], consistent with the thermochronological models that predict cooling through 400°C at *c*. 12–13 Ma [*Boutonnet et al*., 2012]. Thus, weakening processes in the leucogranites began to operate <2 Ma after the initiation of faulting on the Tangtse strand.

[60] Tourmaline veins on the Tangtse strand are inferred to postdate the main phase of ductile deformation. As on the Nubra strand, they provide evidence for fluid overpressure and hydrofracturing once the rocks had been exhumed to shallower crustal levels. Other brittle structures within the Tangtse strand such as shear fractures in leucogranite and marble cataclasites show that the fault strand continued to be a zone of relative weakness following exhumation and cooling to <250–300°C (<8–10 km depth).

4.3. Weakening Mechanisms on the Arganglas Fault Strand

[61] Metapelites of the Saser Formation within the Arganglas fault strand contain a high proportion of aligned biotite (<50%). The abundance and low frictional strength ($\mu = 0.25$–0.40) of biotite would have resulted in low shear strength of the bulk rock. Deformed quartz veins within the metapelites again suggest elevated pore fluid pressures during deformation; although on the Arganglas strand, they cannot be conclusively demonstrated to be synkinematic with respect to the KFZ. This deformation occurred at depths of 15–18 km (Figure 8) and postdates emplacement of the *c*. 16 Ma Nubra-Siachen leucogranite [*Phillips et al*., 2004, *Phillips and Searle*, 2007]. Undeformed pods of metapelite within marble provide evidence for the weakness of the metapelite relative to the marble. Marble breccias and cataclasites indicate that the Arganglas strand continued to represent a zone of relative weakness following exhumation and cooling to <250–300°C (<8–10 km depth).

4.4. The Pangong Fault Strand

[62] The Pangong fault strand is the fourth major strand of the KFZ in the study area and runs parallel to the Tangtse strand (Figure 2). Between Muglib and Pangong Lake, the Pangong strand cuts primarily through marbles of the Pangong Metamorphic Complex. The comparative lack of phyllosilicate-rich lithologies in this portion of the fault indicates that it would likely be relatively strong. Calcite twinning incidence and calcite recrystallized grain size palaeopiezometry indicate stresses of <250 MPa and 40–110 MPa, respectively [*Rutter et al*., 2007]. The twinning incidence result of <250 MPa shows that for at least part of its lifespan, the Pangong strand sustained high differential stresses in the region of the FVTZ. However, the deformed marbles are crosscut by a later <10 m wide gouge zone-bearing chlorite, muscovite, and illite (along with quartz, calcite and minor dolomite, microcline, saponite, and gypsum) that, based on the illite Kübler index, formed at *c*. 300°C [*Rutter et al*., 2007]. This estimate overlaps with the likely temperatures at which calcite develops twins and so may reflect an evolution from a strong fault to a potentially weaker phyllosilicate-rich zone of deformation (Figure 8). Such an interpretation is supported by recent experimental results from chlorite, muscovite/illite, and saponite-bearing gouges from the Alpine Fault, New Zealand, which found that the gouges deformed with low coefficients of sliding friction in the range 0.28–0.37 and exhibited velocity strengthening behavior [*Barth et al*., 2013; *Boulton et al*., 2012]. According to the cooling model of *Boutonnet et al*. [2012] for the Pangong strand (their "Muglib strand"), cooling through 300°C occurred at *c*. 7 Ma. This date is proposed therefore for the time at which the Pangong strand may have begun to behave with a reduced coefficient of friction.

4.5. Hydraulic Characteristics of the Nubra Fault Strand

[63] The impact of pore fluids on frictional rock shear strength depends on whether pore fluid pressures can be sustained at elevated levels. Sustained high fluid pressures reduce the effective normal stress on fractures and promote slip at reduced values of shear stress. However, open fractures potentially create sufficient permeability for fluids to remain at relatively low hydrostatic pressures [*Townend and Zoback*, 2000]. These opposing effects are controlled in part by the bulk behavior of the fault zone, either as a conduit or a barrier to fluid flow [*Caine et al*., 1996], and in part by the effect of those fluids in causing fracture-induced permeability or permeability reduction by cement precipitation [e.g., *Collettini and Holdsworth*, 2004].

[64] The exposed lithologies on the Nubra fault strand provide an opportunity to examine the hydraulic characteristics of the fault. In the fault core, foliated cataclasites would likely act as a barrier to fluid flow at the depths of the FVTZ. The observed tourmaline ± quartz veins and travertine deposits, inferred to have formed at shallower depths, together with present-day hydrothermal springs on the fault

trace, show that abundant fluid flow occurs in the brittle regime. In the less intensely deformed leucogranites, microfracturing associated with sericitization of feldspars, along with multiple generations of tourmaline ± quartz veins [*Watkins*, 2011], indicates that the fault damage zone largely acted as a conduit for fluid flow. Repeated fracturing and sealing during formation of the tourmaline ± quartz veins indicate cyclicity in pore fluid pressure buildup, leading to microfracturing [*Watkins*, 2011]. These observations suggest that the Nubra fault strand may be classified (in the sense of *Caine et al*. [1996]) as a distributed conduit at shallow levels, transitioning to a combined conduit-barrier to hydrous and boron-rich fluids at depths approaching the FVTZ. Boron within the tourmaline was likely sourced from the metasedimentary lithologies, as recognized in other metasomatic intrusive settings [e.g., *Corteel and De Paepe*, 2003]. Precipitation of tourmaline ± quartz veins and travertine within this system acted to occlude permeability, leading to elevated pore fluid pressures, and resulting in hydrofracture. Thus, it is possible that effective fracture sealing, particularly in the fault core, could have led to deformation at low values of shear stress.

[65] At depths of 10–13 km, phyllonitization resulting from hydrous retrograde mineral reactions affected a *c*. 10 m wide band of the Nubra Formation. This suggests therefore that the fault acted as a distributed conduit within this zone at these depths. At the somewhat greater depths of 13–18 km, sericitization affected the leucogranites across a zone several hundred meters in width. The fault acted therefore as a widely distributed conduit at these depths.

4.6. Seismogenic Potential of the KFZ

[66] The operation of fault weakening mechanisms on some faults has been suggested to promote aseismic creep at the expense of generating large earthquakes. These mechanisms include the presence of weak mineral phases (San Andreas fault, *Carpenter et al*. [2011]), interconnected weak layers of phyllosilicates (Zuccale fault, *Collettini et al*. [2009]) and fluid overpressure [*Byerlee*, 1990], all of which are evident in the KFZ. Faults that are creeping at shallow crustal levels show a distinctive displacement discontinuity in InSAR data [e.g., *Bürgmann et al*., 2000; *Lyons and Sandwell*, 2003]. The KFZ, however, lacks this distinctive signature [*Wang and Wright*, 2012; *Wright et al*., 2004] showing that it is not creeping at shallow depths. Rather, the InSAR data show that the fault is currently accumulating displacement at *c*. 5 mm/yr in its central portion but that this is distributed over a broad region, consistent with the seismogenic layer being fully locked [*Wang and Wright*, 2012].

[67] Fault scaling relationships show that moment magnitude (M) 7 and 8 earthquakes on strike-slip faults typically produce displacements of *c*. 1 m and 10 m, respectively (*Wells and Coppersmith*, 1994). Thus, the 120 km offset accumulated on the KFZ over 15 Ma [*Phillips et al*., 2004; *Phillips et al*., 2013, *Searle et al*., 2011] could be produced by M7 earthquakes with 125 year average recurrence intervals or M8 earthquakes with 1250 year average recurrence intervals. *Brown et al*. [2002] utilized ^{10}Be dating of an offset debris flow on the Pangong strand to determine that 2–2.5 m offset had occurred in the last 1–2 kyr and suggested that it resulted from a single earthquake. This offset would typically require a *c*. M7.5 earthquake on a strike-slip fault [*Wells and Coppersmith*, 1994]. *Brown et al*. [2002] also report an 11–14 ka debris flow offset by 40 ± 5 m, which would require such M7.5 events to occur with a recurrence interval in the range 488–1000 years. These recent and long-term considerations suggest that the seismicity on the KFZ may be characterized by *c*. M7.5+ events with recurrence intervals of the order of 1000 years. This is the same as the seismogenic potential calculated from the regional stress and strain field [*Houlié and Phillips*, 2013]. Coulomb stress modeling suggests that the rupture history of the KFZ may be modulated by seismic activity along the subduction plane of the Indian plate to the SW [*Houlié and Phillips*, 2013].

[68] These characteristics, of a fault showing potential for frictional weakness but also seeming to deform by large magnitude earthquakes, are remarkably similar to observations on the southern onshore portion of the Alpine Fault. There, frictionally weak (steady-state friction coefficients 0.12–0.37), velocity strengthening fault core gouges (expected to deform by slow aseismic slip) are associated with a palaeoseismic record of large magnitude earthquakes over the last 8000 years [*Barth et al*., 2013 and references therein]. This was attributed in large part to switches between velocity strengthening/weakening behavior with increasing temperature in a variety of materials, along with variable rheological behavior resulting from varied mineral proportions, fault roughness, pore fluid pressure fluctuations, and competing deformation mechanisms [*Barth et al*., 2013]. The results of this study suggest that all of these may be important factors also impacting seismicity on the KFZ, making it difficult to infer the seismic nature of the fault from study of the exposed fault rocks alone.

4.7. Frictional Heating on the KFZ

[69] It has been suggested that frictional heating on the KFZ may have led to synkinematic metamorphism and anatexis [*Lacassin et al*., 2004a, 2004b; *Rolland et al*., 2009; *Valli et al*., 2007, 2008]. This suggestion was considered as evidence that the KFZ has a high slip rate over geological timescales and is lithospheric in scale, allowing it to accommodate eastward extrusion of Tibet in a plate-like manner [*Lacassin et al*., 2004a, 2004b; *Rolland and Pêcher*, 2001]. However, this interpretation has been contested on the grounds that not only do peak metamorphism [*Streule et al*., 2009] and anatexis [*Phillips et al*., 2013] predate the fault zone, but also are widespread in occurrence away from the KFZ and hence were not produced by the KFZ [*Phillips et al*., 2004; *Phillips and Searle*, 2007; *Searle et al*., 1990, 1998; *Searle and Phillips*, 2004]. The potential for the KFZ to have deformed with a reduced coefficient of friction documented in this study makes it unlikely that the fault could have generated significant shear heating, particularly given its low slip rate [*LeLoup et al*., 1999]. Further, the evidence for fluid flow at variable crustal depths indicates that any frictional heat generated would be advected toward the surface, as is happening today by hydrothermal systems, making it unlikely that the temperatures could be significantly raised due to faulting. This is supported by the observations of retrograde greenschist facies assemblages in the phyllonites and sericitization in the granites, which show that the deformation was associated with retrograde rather than prograde metamorphism. Concomitantly, crustal thickening is likely responsible for the prograde metamorphism and anatexis of the extensive Karakoram Metamorphic Complex of the

Asian margin [*Leloup et al*., 2011; *Searle et al*., 2010]. The findings of this study support the conclusion that the KFZ has not generated significant shear heating.

4.8. Fault Weakening and Implications for Continental Lithospheric Strength

[70] Studies into the characteristics of continental deformation have tried to determine the main load-bearing depth range within the continental lithosphere [*Chen et al*., 2012; *Hirth and Kohlstedt*, 2003; *Jackson*, 2002]. Various models have been put forward in which the maximum lithospheric strength resides in the upper crust, lower crust, or upper lithospheric mantle [*Bürgmann and Dresen*, 2008; *Burov*, 2011]. A prediction of models for which the crust is the strongest portion of the lithosphere is that deformation will be accommodated on a small number of laterally extensive and narrow faults that penetrate the entire crust with high slip rates and shear heating [e.g., *Avouac and Tapponnier*, 1993]. Such faults would be capable of accommodating plate-like motion of fault-bounded rigid crustal blocks and in the Himalayan-Tibetan orogen are used to support plate-like motion of Tibet [*Peltzer and Tapponnier*, 1988]. If such a fault zone slipped with a much reduced coefficient of friction ($\mu < 0.4$), it would exhibit large offsets and high slip rates due to the reduced resistance [*He and Chéry*, 2008] but would not cause significant shear heating. The KFZ has previously been demonstrated to have a fairly low offset (40–150 km) [*Gaudemer et al*., 1989; *Searle*, 1996; *Wang et al*., 2012] and low slip rate ($\leq$10 mmyr^{1}) [*Brown et al*., 2005; *Chevalier et al*., 2012; *England and Molnar*, 2005; *Meade*, 2007; *Molnar and Lyon-Caen*, 1989; *Phillips et al*., 2004; *Wang and Wright*, 2012], making it unlikely to have played a major role in accommodating plate-like motion of Tibet [*Searle et al*., 2011]. Evidence for the potential weakness of the KFZ strengthens this argument as, even with a potentially low coefficient of friction; it has only a limited offset and low slip rate, making only a limited contribution to plate-like deformation of the Asian crust. The low offset and slip rate, even on a potentially weak fault, argues that the main load-bearing region of the lithosphere must be beneath the depth of penetration of the fault and lie within the lower crust or upper mantle. Such a situation would occur in the presence of dry rocks dominated by either feldspar in the lower crust or olivine in the lithospheric mantle [*Bürgmann and Dresen*, 2008; *Jackson*, 2002] and is inconsistent with models where continental lithospheric strength is concentrated in the upper crust [*Jackson*, 2002].

5. Conclusions

[71] Fault rocks presently exposed along the KFZ in Ladakh, NW Himalaya, record deformation at depths spanning the FVTZ and reveal evidence for the operation of several fault weakening mechanisms, including exploitation of preexisting weak mineral phases, reaction softening, interconnected weak layer development, and high pore fluid pressures. These suggest that the KFZ has had potential to act as a weak fault, deforming with significantly less than Byerlee friction. These weakening mechanisms are likely to have operated in the exposed structural level since at least 14–15 Ma and may continue to do so at depth.

[72] The fault rocks exposed along the KFZ provide field examples of fault rocks in which experimentally predicted fault weakening mechanisms such as frictional-viscous deformation may have operated. Additionally the KFZ can be regarded as an analogue for other potentially weak active strike-slip fault zones where such weakening mechanisms may be active at depth. Unlike some faults where weakening has been associated with aseismic creep or small earthquakes, the KFZ is currently fully locked and likely generates M7–8 earthquakes with *c*. 1000 year recurrence intervals.

[73] The operation of low friction deformation mechanisms within the KFZ, coupled with thermal advection by fluids, makes it unlikely that shear heating could have significantly raised midcrustal temperatures to result in peak metamorphism and anatexis in the fault zone. Instead, high grade metamorphic rocks and migmatites are likely the result of orogenic crustal thickening, in accord with their widespread occurrence across the Karakoram. Fault-related metamorphism on the other hand is retrogressive sericitization and phyllonitization.

[74] If the KFZ does indeed act as a weak fault, then its low slip rate and limited offset suggest that the long-term strength of the lithosphere in this region occurs beneath the depths where weakening processes operate, in the lower crust or lithospheric mantle. These observations demonstrate the need to consider fault zone strength when assessing the role of faults in accommodating orogenic deformation.

[75] **Acknowledgments.** We are grateful to Fida Hussain Mitoo of the New Royal Guest House, Leh, for logistical support in Ladakh. Andrew Parsons and Hannah Watkins are thanked for assistance during fieldwork. We also thank Onno Oncken, Jonathan Imber, and Virginia Toy and for their detailed and constructive comments that helped to greatly improve the manuscript. DW gratefully acknowledges support from NERC (training grant NE/I528750/1).

References

Absar, A., G. Prakash, and R. K. Aggarwal (1991), A Preliminary Conceptual Model of Nubra Valley Geothermal System, Ladakh, J and K, India, *J. Geol. Soc. India*, *37*, 533–545.

Avouac, J.-P., and P. Tapponnier (1993), Kinematic model of active deformation in central Asia, *Geophys. Res. Lett.*, *20*, 895–898.

Barth, N. V., C. J. Boulton, B. M. Carpenter, G. E. Batt, and V. G. Toy (2013), Slip localization on the southern Alpine Fault, New Zealand, *Tectonics*, *32*, 620–640, doi:10.1002/tect.20041.

Bhutani, R., K. Pande, and N. Desai (2003), Age of the Karakoram fault activation: ^{40}Ar-^{39}Ar geochronological study of Shyok suture zone in northern Ladakh, India, *Curr. Sci.*, *84*, 1454–1458.

Blacic, J. D., and J. M. Christie (1984), Plasticity and Hydrolytic Weakening of Quartz Single Crystals, *J. Geophys. Res.*, *89*, 4223–4239.

Bos, B., and C. J. Spiers (2001), Experimental investigation into the microstructural and mechanical evolution of phyllosilicate-bearing fault rock under conditions favouring pressure solution, *J. Struct. Geol.*, *23*, 1187–1202.

Bos, B., and C. J. Spiers (2002), Frictional-viscous flow of phyllosilicate-bearing fault rock: Microphysical models and implications for crustal strength profiles, *J. Geophys. Res.*, *107*(B2), 2028, doi:10.1029/2011JB000301.

Boulton, C., B. M. Carpenter, V. Toy, and C. Marone (2012), Physical properties of surface outcrop cataclastic fault rocks, Alpine Fault, New Zealand, *Geochem. Geophys. Geosyst.*, *13*, Q01018, doi:10.1029/2011GC003872.

Boutonnet, E., P. H. Leloup, N. Arnaud, J.-L. Paquette, W. J. Davis, and K. Hattori (2012), Synkinematic magmatism, heterogeneous deformation, and progressive strain localization in a strike-slip shear zone: The case of the right-lateral Karakorum fault, *Tectonics*, *31*, TC4012, doi:10.1029/2011TC003049.

Brodie, K. H., and E. H. Rutter (1985), On the relationship between deformation and metamorphism, with special reference to the behaviour of basic rocks, in *Kinetics, Textures and Deformation, Advances in Physical*

Geochemistry, vol. 4, edited by A. B. Thompson and D. Rubie, pp. 138–179, Springer, New York.

Brown, E. T., R. Bendick, D. L. Bourles, V. Gaur, P. Molnar, G. M. Raisbeck, and F. Yiou (2002), Slip rates of the Karakoram Fault, Ladakh, India, determined using cosmic ray exposure dating of debris flows and moraines, *J. Geophys. Res.*, *107*(B9), 2192, doi:10.1029/2000JB000100.

Brown, E., P. Molnar, and D. L. Bourles (2005), Comment on Chevalier *et al*., 2005 'Slip rate measurements on the Karakoram fault may imply secular variations in fault motion', *Science*, *309*, 1326.

Burkhard, M. (1993), Calcite twins, their geometry, appearance and significance as stress–strain markers and indicators of tectonic regime: A review, *J. Struct. Geol.*, *15*, 351–368.

Bürgmann, R., D. Schmidt, R. M. Nadeau, M. d'Alessio, E. Fielding, D. Manaker, T. V. McEvilly, and M. H. Murray (2000), Earthquake Potential Along the Northern Hayward Fault, California, *Science*, *289*, 1178–1182.

Bürgmann, R., and G. Dresen (2008), Rheology of the Lower Crust and Upper Mantle: Evidence from Rock Mechanics, Geodesy, and Field Observations, *Annu. Rev. Earth Planet. Sci.*, *36*, 531–567.

Burov, E. B. (2011), Rheology and strength of the lithosphere, *Mar. Pet. Geol.*, *28*, 1402–1443.

Byerlee, J. (1978), Friction of Rocks, *Pure Appl. Geophys.*, *116*(4–5), 615–626.

Byerlee, J. (1990), Friction, overpressure and fault normal compression, *Geophys. Res. Lett.*, *17*, 2109–2112.

Caine, J. S., J. P. Evans, and C. B. Forster (1996), Fault zone architecture and permeability structure, *Geology*, *24*(11), 1025–1028.

Carpenter, B. M., C. Marone, and D. M. Saffer (2011), Weakness of the San Andreas Fault Revealed by samples from the active fault zone, *Nat. Geosci.*, *4*, 251–254.

Chen, W. P., S. H. Hung, T. L. Tseng, M. Brudzinski, Z. H. Yang, and R. L. Nowack (2012), Rheology of the continental lithosphere: Progress and new perspectives, *Gondwana Research*, *21*(1), 4–18.

Chester, F. M. (1995), A rheologic model for wet crust applied to strike-slip faults, *J. Geophys. Res.*, *100*, 13,033–13,044.

Chester, F. M., and J. S. Chester (1998), Ultracataclasite structure and friction processes of the Punchbowl fault, San Andreas system, California, *Tectonophysics*, *295*, 199–221.

Chester, F. M., and N. G. Higgs (1992), Multimechanism friction constitutive model for ultrafine quartz gouge at hypocentral conditions, *J. Geophys. Res.*, *97*, 1859–1870.

Chester, F. M., and J. M. Logan (1986), Implications for mechanical properties of brittle faults from observations of the Punchbowl Fault, California, *Pure Appl. Geophys.*, *124*, 79–106.

Chevalier, M.-L., P. Tapponnier, J. Van der Woerd, F. J. Ryerson, R. C. Finkel, and H. B. Li (2012), Spatially constant slip rate along the southern segment of the Karakorum fault since 200 Ka, *Tectonophysics*, *530*, 152–179.

Collettini, C., A. Niemeijer, C. Viti, and C. Marone (2009), Fault zone fabric and fault weakness, *Nature*, *462*, 907–910.

Collettini, C., and R. E. Holdsworth (2004), Fault zone weakening and character of slip along low-angle normal faults: Insights from the Zuccale fault, Elba, Italy, *J. Geol. Soc. London*, *161*, 1039–1051.

Collettini, C., N. De Paola, R. E. Holdsworth, and M. R. Barchi (2006), The development and behaviour of low-angle normal faults during Cenozoic asymmetric extension in the Northern Apennines, Italy, *J. Struct. Geol.*, *28*, 333–352.

Cook, K. L., and L. H. Royden (2008), The role of crustal strength variations in shaping orogenic plateaus, with application to Tibet, *J. Geophys. Res.*, *113*, B08407, doi:10.1029/2007JB005457.

Corteel, C., and P. De Paepe (2003), Boron metasomatism in the Brabant Massif (Belgium): Geochemical and petrographical evidence of Devonian tourmalinite pebbles, *Neth. J. Geosci.-Geologie En Mijnbouw*, *82*, 197–208.

De Bresser, J. H. P., J. H. Ter Heege, and C. J. Spiers (2001), Grain size reduction by dynamic recrystallisation: Can it result in major rheological weakening?, *Int. J. Earth Sci.*, *90*, 28–45.

Dewers, T., and P. Ortoleva (1991), Influences of clay minerals on sandstone cementation and pressure solution, *Geology*, *19*, 1045–1048.

Di Toro, G., R. Han, T. Hirose, N. De Paola, S. Nielsen, K. Mizoguchi, F. Ferri, M. Cocco, and T. Shimamoto (2011), Fault lubrication during earthquakes, *Nature*, *471*, 494–498.

Dunlap, W. J., R. F. Weinberg, and M. P. Searle (1998), Karakoram fault zone rocks cool in two phases, *J. Geol. Soc. London*, *155*, 903–912.

Eberl, D. D., J. Srodon, M. Lee, and P. H. Nadeau (1987), Sericite from the Silverton caldera, CO: Correlation among structure, composition, origin, and particle thickness, *Am. Mineral.*, *72*, 914–935.

England, P., and P. Molnar (2005), Late Quaternary to decadal velocity fields in Asia, *J. Geophys. Res.*, *110*, B12401, doi:10.1029/2004JB003541.

Faulkner, D. R., A. C. Lewis, and E. H. Rutter (2003), On the internal structure and mechanics of large strike-slip fault zones: field observations of the Carboneras fault in southeastern Spain, *Tectonophysics*, *367*, 235–251.

Gaudemer, Y., P. Tapponnier, and D. L. Turcotte (1989), River offsets across active strike-slip faults, *Annales Tectonicae*, *3*, 55–76.

Handy, M. R. (1990), Solid State Flow of Polymineralic Rocks, *J. Geophys. Res.*, *95*, 8647–8661.

Handy, M. R., S. B. Wissing, and L. S. Streit (1999), Frictional-viscous flow in mylonite with varied bimineralic composition and its effect on lithospheric strength, *Tectonophysics*, *303*, 175–191.

Harrison, T. M., I. Duncan, and I. McDougall (1985), Diffusion of ^{40}Ar in biotite: Temperature, pressure and compositional effects, *Geochim. Cosmochim. Ac.*, *49*, 2461–2468.

He, J., and J. Chéry (2008), Slip rates of the Altyn Tagh, Kunlun and Karakorum faults (Tibet) from 3D mechanical modelling, *Earth Planet. Sci. Lett.*, *274*, 50–58.

Hickman, S. H., and B. Evans (1995), Kinetics of pressure solution at halite-silica interfaces and intergranular clay films, *J. Geophys. Res.*, *100*, 13,113–13,132.

Hippertt, J. F. M. (1994), Grain boundary microstructures in micaceous quartzite: Significance for fluid movement and deformation processes in low metamorphic grade shear zones, *Geology*, *102*, 331–348.

Hirth, G., and D. Kohlstedt (2003), Rheology of the upper mantle and the mantle wedge: A view from the experimentalists, in *Inside the Subduction Factory*, Geophysical Monograph, vol. 138, edited by J. Eiler, pp. 83–105, American Geophysical Society, Washington, D.C.

Hirth, G., and J. Tullis (1994), The brittle-plastic transition in experimentally deformed quartz aggregates, *J. Geophys. Res.*, *99*, 11,731–11,747.

Holdsworth, R. E. (2004), Weak Faults-Rotten Cores, *Science*, *303*, 181–182.

Houlié, N., and R. J. Phillips (2013), Quaternary rupture behaviour of the Karakoram Fault and its relation to the dynamics of the continental lithosphere, NW Himalaya-Western Tibet, *Tectonophysics*, doi:10.1016/j.tecto.2013.03.029.

Houseknecht, D. W. (1988), Intergranular pressure solution in four quartzose sandstones, *J. Sediment. Petrol.*, *58*, 228–246.

Ikari, M. J., C. Marone, and D. M. Saffer (2011), On the relation between fault strength and frictional stability, *Geology*, *39*, 83–86, doi:10.1130/G31416.1.

Imber, J., R. E. Holdsworth, C. A. Butler, and R. A. Strachan (2001), A reappraisal of the Sibson-Scholz fault zone model: The nature of the frictional to viscous ("brittle-ductile") transition along a long-lived, crustal-scale fault, Outer Hebrides, Scotland, *Tectonics*, *20*, 601–624.

Imber, J., R. E. Holdsworth, S. A. F. Smith, S. P. Jefferies, and C. Collettini (2008), Frictional-viscous flow, seismicity and the geology of weak faults: A review and future directions, *Geol. Soc. London Spec. Publ.*, *299*, 151–173.

Jackson, J. (2002), Strength of the continental lithosphere: Time to abandon the jelly sandwich?, GSA Today, September, 4–10.

Jefferies, S. P., R. E. Holdsworth, T. Shimamoto, H. Takagi, G. E. Lloyd, and C. J. Spiers (2006a), Origin and mechanical significance of foliated cataclastic rocks in the cores of crustal scale faults: Examples from the Median Tectonic Line, Japan, *J. Geophys. Res.*, *111*, B12303, doi:10.1029/2005JB004205.

Jefferies, S. P., R. E. Holdsworth, C. A. J. Wibberley, T. Shimamoto, C. J. Spiers, A. R. Niemeijer, and G. E. Lloyd (2006b), The nature and importance of phyllonite development in crustal-scale fault cores: An example from the Median Tectonic Line, Japan, *J. Struct. Geol.*, *28*, 220–235.

Kirstein, L. A., J. P. T. Foeken, P. Van der Beek, F. M. Stuart, and R. J. Phillips (2009), Cenozoic unroofing history of the Ladakh Batholith, western Himalaya, constrained by thermochronology and numerical modelling, *J. Geol. Soc. London*, *166*, 667–678.

Klemperer, S. L., B. M. Kennedy, S. R. Sastry, Y. Makovsky, T. Harinarayana, and M. L. Leech (2013), Mantle fluids in the Karakoram fault: Helium isotope evidence, *Earth Planet. Sci. Lett.*, doi:10.1016/j.epsl.2013.01.013.

Lacassin, R., et al. (2004a), Large-scale geometry, offset and kinematic evolution of the Karakoram Fault, Tibet, *Earth Planet. Sci. Lett.*, *219*, 255–269.

Lacassin, R., et al. (2004b), Reply to Comment on "Large-scale geometry, offset and kinematic evolution of the Karakoram fault, Tibet", *Earth Planet. Sci. Lett.*, *229*, 159–163.

Leloup, P. H., E. Boutonnet, W. J. Davis, and K. Hattori (2011), Long-lasting intracontinental strike-slip faulting: New evidence from the Karakoram shear zone in the Himalayas, *Terra Nova*, *23*, 92–99.

Leloup, P. H., Y. Ricard, J. Battaglia, and R. Lacassin (1999), Shear heating in continental strike-slip shear zones: Model and field examples, *Geophys. J. Int.*, *136*, 19–40.

Lyons, S., and D. Sandwell (2003), Fault creep along the southern San Andreas from interferometric synthetic aperture radar, permanent

scatterers, and stacking, *J. Geophys. Res.*, *108*(B1), 2047, doi:10.1029/2002JB001831.
Meade, B. J. (2007), Present-day kinematics at the India-Asia collision zone, *Geology*, *35*, 81–84.
Molnar, P., and H. Lyon-Caen (1989), Fault plane solutions of earthquakes and active tectonics of the Tibetan Plateau and its margins, *Geophys. J. Int.*, *99*, 123–153.
Morrow, C. A., D. E. Moore, and D. A. Lockner (2000), The effect of mineral bond strength and adsorbed water on fault gouge frictional strength, *Geophys. Res. Lett.*, *27*, 815–818.
Mukherjee, B. K., K. Sen, H. K. Sachan, and S. K. Paul (2012), Exhumation history of the Karakoram fault zone mylonites: New constraints from microstructures, fluid inclusions, and Ar-40-Ar-39 analyses, *Lithosphere*, *4*, 230–241.
Murphy, M. A., A. Yin, P. Kapp, T. M. Harrison, L. Ding, and J. Gou (2000), Southward propagation of the Karakoram fault system, southwest Tibet: Timing and magnitude of slip, *Geology*, *28*, 451–454.
Niemeijer, A. R., and C. J. Spiers (2005), Influence of phyllosilicates on fault strength in the brittle-ductile transition: insights from rock analogue experiments, in *High Strain Zones: Structure and Physical Properties*, vol. 245, edited by D. Bruhn and L. Burlini, pp. 303–327, Geological Society, London, Special Publications, Bath, UK.
Palin, R. M., M. P. Searle, D. J. Waters, M. S. A. Horstwood, and R. R. Parrish (2012), Combined thermobarometry and geochronology of peraluminous metapelites from the Karakoram metamorphic complex, North Pakistan; New insight into the tectonothermal evolution of the Baltoro and Hunza Valley regions, *J. Metamorph. Geol.*, *30*, 793–820.
Peltzer, G., and P. Tapponnier (1988), Formation and evolution of strike-slip faults, rifts, and basins during the India-Asia collision: An experimental approach, *J. Geophys. Res.*, *93*, 15,085–15,117.
Phillips, R. J. (2008), Geological map of the Karakoram Fault zone, Eastern Karakoram, Ladakh, NW Himalaya, *J. Maps*, *2008*, 38–49, doi:10.4113/jom.2008.93.
Phillips, R. J., R. R. Parrish, and M. P. Searle (2004), Age constraints on ductile deformation and long-term slip rates along the Karakoram fault zone, Ladakh, *Earth Planet. Sci. Lett.*, *226*, 305–319.
Phillips, R. J., and M. P. Searle (2007), Macrostructural and microstructural architecture of the Karakoram fault: Relationship between magmatism and strike-slip faulting, *Tectonics*, *26*, TC3017, doi: 10.1029/2006TC001946.
Phillips, R. J., M. P. Searle, and R. R. Parrish (2013), The geochemical and temporal evolution of the continental lithosphere and its relationship to continental-scale faulting: The Karakoram Fault, Eastern Karakoram, NW Himalaya, *Geochem., Geophys., Geosyst.*, *14*, 1525–2027, doi:10.1002/ggge.20061.
Que, M., and A. R. Allen (1996), Sericitization of plagioclase in the Rosses Granite Complex, Co. Donegal, Ireland, *Mineral. Mag.*, *60*, 927–936.
Reichardt, H., and R. F. Weinberg (2012), Hornblende Chemistry in Meta- and Diatexites and its Retention in the Source of Leucogranites: An Example from the Karakoram Shear Zone, NW India, *J. Petrol.*, *53*, 1287–1318.
Reichardt, H., R. F. Weinberg, U. B. Andersson, and C. M. Fanning (2010), Hybridization of granitic magmas in the source: The origin of the Karakoram Batholith, Ladakh, NW India, *Lithos*, *116*, 249–272.
Robinson, A. C. (2009), Geologic offsets across the northern Karakorum fault: Implications for its role and terrane correlations in the western Himalayan-Tibetan orogen, *Earth Planet. Sci. Lett.*, *279*, 123–130.
Rolland, Y., G. Maheo, A. Pêcher, and I. Villa (2009), Syn-kinematic emplacement of the Pangong metamorphic and magmatic complex along the Karakoram Fault (north Ladakh), *J. Asian Earth Sci.*, *34*, 10–25.
Rolland, Y., and A. Pêcher (2001), The Pangong granulites of the Karakoram Fault (Western Tibet): Vertical extrusion within a lithospheric scale fault?, *C. R. Acad. Sci.*, *332*, 363–370.
Rutter, E. H., D. R. Faulkner, K. H. Brodie, R. J. Phillips, and M. P. Searle (2007), Rock deformation processes in the Karakoram fault zone, Eastern Karakoram, Ladakh, NW India, *J. Struct. Geol.*, *29*, 1315–1326.
Rutter, E. H., R. E. Holdsworth, and R. J. Knipe (2001), The nature and tectonic significance of fault-zone weakening: An introduction, in *The Nature and Tectonic Significance of Fault Zone Weakening*, vol. 186, edited by R. E. Holdsworth, R. A. Strachan, J. F. Magloughlin, and R. J. Knipe, pp. 1–11, The Geological Society, London, Special Publication, Bath, UK.
Saffer, D. M., K. M. Frye, C. Marone, and K. Mair (2001), Laboratory results indicating complex and potentially unstable frictional behaviour of smectite clay, *Geophys. Res. Lett.*, *28*, 2297–2300.
Scholz, C. H. (1998), Earthquakes and friction laws, *Nature*, *391*, 37–42.
Scruggs, V. J., and T. E. Tullis (1998), Correlation between velocity dependence of friction and strain localization in large displacement experiments on feldspar, muscovite and biotite gouge, *Tectonophysics*, *295*, 15–40.
Searle, M. P. (1996), Geological evidence against large-scale pre-Holocene offsets along the Karakoram Fault: Implications for the limited extrusion of the Tibetan Plateau, *Tectonics*, *15*, 171–186.
Searle, M. P., J. R. Elliott, R. J. Phillips, and S.-L. Chung (2011), Crustal-lithospheric structure and continental extrusion of Tibet, *J. Geol. Soc. London*, *168*, 633–672, doi:10.1144/0016-76492010-139.
Searle, M. P., R. R. Parrish, A. V. Thow, S. R. Noble, R. J. Phillips, and D. J. Waters (2010), Anatomy, age and evolution of a collisional mountain belt: The Baltoro granite batholith and Karakoram Metamorphic Complex, Pakistani Karakoram, *J. Geol. Soc. London*, *167*, 183–202.
Searle, M. P., R. R. Parrish, R. Tirrul, and D. C. Rex (1990), Age of crystallisation and cooling of the K2 gneiss in the Baltoro Karakoram, *J. Geol. Soc. London*, *147*, 603–606.
Searle, M. P., and R. J. Phillips (2004), A comment on 'Large-scale geometry, offset and kinematic evolution of the Karakoram Fault, Tibet', *Earth Planet. Sci. Lett.*, *229*, 155–158.
Searle, M. P., and R. J. Phillips (2007), Relationships between right-lateral shear along the Karakoram fault and metamorphism, magmatism, exhumation and uplift: Evidence from the K2-Gasherbrum-Pangong ranges, north Pakistan and Ladakh, *J. Geol. Soc.*, *164*, 439–450.
Searle, M. P., R. F. Weinberg, and W. J. Dunlap (1998), Transpressional tectonics along the Karakoram fault zone, northern Ladakh: constraints on Tibetan extrusion, in *Continental Transpressional and Transtensional Tectonics*, vol. 35, edited by R. E. Holdsworth, R. A. Strachan, and J. F. Dewey, pp. 307–326, Geological Society, London, Special Publications, Bath, UK.
Smith, S. A. F., C. Collettini, and R. E. Holdsworth (2008), Recognizing the seismic cycle along ancient faults: CO_2-induced fluidization of breccias in the footwall of a sealing low-angle normal fault, *J. Struct. Geol.*, *30*, 1034–1046.
Steffen, K., J. Selverstone, and A. Brearley (2001), Episodic weakening and strengthening during synmetamorphic deformation in a deep-crustal shear zone in the Alps, in *The Nature and Tectonic Significance of Fault Zone Weakening*, vol. 186, edited by R. E. Holdsworth et al., pp. 141–156, Geological Society, London, Special Publications, Bath, UK.
Stewart, M., R. E. Holdsworth, and R. A. Strachan (2000), Deformation processes and weakening mechanisms within the frictional-viscous transition zone of major crustal-scale faults: Insights from the Great Glen Fault Zone, Scotland, *J. Struct. Geol.*, *22*, 543–560.
Stipp, M., H. Stünitz, R. Heilbronner, and S. M. Schmid (2002), Dynamic recrystallization of quartz: Correlation between natural and experimental conditions, in *Deformation Mechanisms, Rheology and Tectonics: Current Status and Future Perspectives*, vol. 20, edited by S. De Meer et al., pp. 171–190, Geological Society, London, Special Publications, Bath, UK.
Streule, M. J., R. J. Phillips, M. P. Searle, D. J. Waters, and M. S. A. Horstwood (2009), Evolution and chronology of the Pangong Metamorphic Complex adjacent to the Karakoram Fault, Ladakh: Constraints from thermobarometry, metamorphic modelling and U Pb geochronology, *J. Geol. Soc.*, *166*, 919–932.
Thakur, V. C., N. S. Virdi, H. Rai, and K. R. Gupta (1981), A Note on the Geology of Nubra-Shyok Area of Ladakh, Kashmir, Himalaya, *J. Geol. Soc. India*, *22*, 46–50.
Townend, J., and M. D. Zoback (2000), How faulting keeps the crust strong, *Geology*, *28*, 399–402.
Tullis, J., and R. A. Yund (1980), Hydrolytic weakening of experimentally deformed Westerly granite and Hale albite rock, *J. Struct. Geol.*, *2*, 439–451.
Tullis, T. E., F. G. Horowitz, and J. Tullis (1991), Flow Laws of Polyphase Aggregates from End-Member Flow Laws, *J. Geophys. Res.*, *96*, 8081–8096.
Valli, F., N. Arnaud, P. H. Leloup, E. R. Sobel, G. Mahéo, R. Lacassin, S. Guillot, H. Li, P. Tapponnier, and Z. Xu (2007), Twenty million years of continuous deformation along the Karakoram fault, western Tibet: A thermochronological analysis, *Tectonics*, *26*, TC4004, doi:10.1029/2005TC001913.
Valli, F., et al. (2008), New U-Th/Pb constraints on timing of shearing and long-term slip-rate on the Karakorum fault, *Tectonics*, *27*, TC5007, doi:10.1029/2007TC002184.
Wang, H., and T. J. Wright (2012), Satellite geodetic imaging reveals internal deformation of western Tibet, *Geophys. Res. Lett.*, *39*, L07303, doi:10.1029/2012GL051222.
Wang, S. C., M. A. Murphy, R. J. Phillips, and C. Wang (2013), Reply to Comment on "Displacement along the Karakoram fault, NW Himalaya, estimated from LA-ICPMS U-Pb dating of offset geologic markers" by Leloup et al. in EPSL, 2012, *Earth Planet. Sci. Lett.*, *363*, 246–248.
Wang, S., C. Wang, R. J. Phillips, M. A. Murphy, X. Fang, and Y. Yue (2012), Displacement along the Karakoram fault, NW Himalaya, estimated from LA-ICP-MS U-Pb dating of offset geologic markers, *Earth Planet. Sci. Lett.*, *337–338*, 156–163.
Watkins, H. E. (2011), Composition and origin of exotic fault-related intrusions, Karakoram fault, Ladakh, NW Himalaya. Unpublished MSc thesis, University of Leeds, UK, pp. 75.
Weinberg, R. F., and G. Mark (2008), Magma migration, folding, and disaggregation of migmatites in the Karakoram Shear Zone, Ladakh, NW India, *Geol. Soc. Am. Bull.*, *120*, 994–1009.

Wells, D. L., and K. J. Coppersmith (1994), New Empirical Relationships among Magnitude, Rupture Length, Rupture Area and Surface Displacement, *Bull. Seismol. Soc. Am.*, *84*, 974–1002.

Wibberley, C. A. J., and T. Shimamoto (2005), Earthquake slip weakening and asperities explained by thermal pressurization, *Nature*, *436*, 689–692.

White, J. C., and S. H. White (1983), Semi-brittle deformation within the Alpine fault zone, New Zealand, *J. Struct. Geol.*, *5*, 579–589.

White, S. H., S. E. Burrows, J. Carreras, N. D. Shaw, and F. J. Humphreys (1980), On mylonites in ductile shear zones, *J. Struct. Geol.*, *2*, 175–187.

Wilson, J. E., J. S. Chester, and F. M. Chester (2003), Microfracture analysis of fault growth and wear processes, Punchbowl Fault, San Andreas system, California, *J. Struct. Geol.*, *25*, 1855–1873.

Wintsch, R. P., R. Christoffersen, and A. K. Kronenberg (1995), Fluid-rock Reaction Weakening of Fault Zones, *J. Geophys. Res.*, *100*, 13,021–13,032.

Wright, T. J., B. Parsons, P. C. England, and E. J. Fielding (2004), InSAR Observations of Low Slip Rates on the Major Faults of Western Tibet, *Science*, *305*, 236–239.

Zhang, R., M. A. Murphy, T. J. Lapen, V. Sanchez, and M. Heizler (2011), Late Eocene crustal thickening followed by Early-Late Oligocene extension along the India-Asia suture zone: Evidence for cyclicity in the Himalayan orogen, *Geosphere*, *7*, 1249–1268, doi:10.1130/GES00643.1.

Zoback, M. D., and H.-P. Harjes (1997), Injection-induced earthquakes and crustal stress at 9 km depth at the KTB deep drilling site, Germany, *J. Geophys. Res.*, *102*, 18,477–18,491.